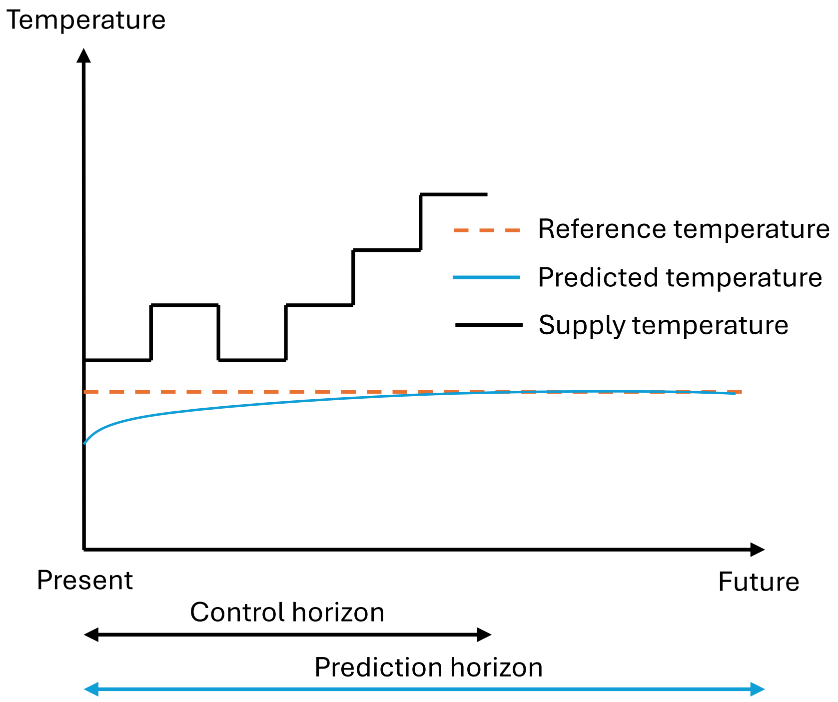

Model predictive control of hydronic heating systems in buildings

Evaluation of energy performance, peak shaving and thermal comfort

Master's thesis in the Master's Programme Structural Engineering and Building Technology

ARVID THEGERSTRÖM
EMIL VENDELSTRAND

DEPARTMENT OF ARCHITECTURE AND CIVIL ENGINEERING
DIVISION OF BUILDING SERVICES ENGINEERING

CHALMERS UNIVERSITY OF TECHNOLOGY
Master's thesis ACEX30
Gothenburg, Sweden 2026

MASTER'S THESIS ACEX30

Model predictive control of hydronic heating systems in buildings

Evaluation of energy performance, peak shaving and thermal comfort

Master's Thesis in the Master's Programme Structural Engineering and Building Technology

ARVID THEGERSTRÖM
EMIL VENDELSTRAND

Department of Architecture and Civil Engineering
Division of Building Services Engineering
CHALMERS UNIVERSITY OF TECHNOLOGY

Gothenburg, Sweden 2026

Model predictive control of hydronic heating systems in buildings
Evaluation of energy performance, peak shaving and thermal comfort
Master's Thesis in the Master's Programme Structural Engineering and Building Technology

ARVID THEGERSTRÖM
EMIL VENDELSTRAND

Industry Supervisors: Gustav Thuresson & Staffan Sjöberg, Ingenjörsbyrån Andersson & Hultmark AB

Academic Supervisor: Torbjörn Lindholm, Department of Architecture and Civil Engineering, Chalmers University of Technology

Examiner: Anders Trüschel, Department of Architecture and Civil Engineering, Chalmers University of Technology

Examensarbete ACEX30
Institutionen för Arkitektur och Samhällsbyggnadsteknik
Chalmers Tekniska Högskola, 2026

Department of Architecture and Civil Engineering
Division of Building Services Engineering
Chalmers University of Technology
SE-412 96 Göteborg
Sweden
Telephone +46 31 772 1000

Cover:
Graph of a basic model predictive controller in a building plotting temperature against time with reference temperature, predicted temperature over the prediction horizon and control sequence for the supply temperature over the control horizon. Further description of figure in Chapter 5.
Department of Architecture and Civil Engineering
Göteborg, Sweden, 2026

Model predictive control of hydronic heating systems in buildings
Evaluation of energy performance, peak shaving and thermal comfort

Master's thesis in the Master's Programme Structural Engineering and Building Technology

ARVID THEGERSTRÖM

EMIL VENDELSTRAND

Department of Architecture and Civil Engineering
Division of Building Services Engineering
Chalmers University of Technology

ABSTRACT

With the increasing need for energy efficiency in the building sector, advanced control strategies might prove to become essential for heating systems. This thesis investigates the implementation and performance of utilizing model predictive control (MPC) to optimize the hydronic heating system's supply temperature in a high complexity, modern office building. The evaluation focuses on energy performance, peak shaving and thermal comfort.

To evaluate the control strategy, a reference building within the advanced building simulation tool IDA ICE was utilized. Since the software does not support model predictive control, a co-simulation was established between IDA ICE and Python. As a predictor for the MPC, simplified resistance capacitance models representing the building zones were constructed.

The simulations were conducted over a two-week period to optimize computational efficiency and in March to evaluate the impact of solar gains. Initially, the results indicated energy savings of 20–30% when implementing the MPC compared to a traditional control system. However, after eliminating temperature discrepancies to ensure a correct comparison, the actual savings related to the control logic were determined to be 3–5%. Regarding peak shaving, the analysis indicated a potential average reduction in peak heating demand of 26% over a one-week period, while indoor thermal comfort was successfully maintained within the defined boundaries of 21–25°C. Furthermore, the robustness of the MPC was tested against forecast uncertainties in outdoor temperature and occupancy. The results demonstrated that the closed-loop feedback effectively compensated for prediction errors and maintained thermal comfort.

Multiple sources of error and limitations were identified. For instance, the results of the shortened two-week simulation period may not apply for other periods of the heating season. Additionally, focusing solely on March presents an idealized scenario since the conditions in March are typically favorable for an MPC due to moderate heating demands and significant solar gains. Nonetheless, the results clearly demonstrate the potential of implementing MPC. While further testing on a physical building is required to validate these findings, MPC offers a viable path forward for enhancing energy efficiency in modern buildings.

Key words: Model predictive control (MPC), Co-simulation, IDA ICE, Resistance capacitance (RC), Peak shaving, Thermal comfort, Energy efficiency

Modellprediktiv styrning av vattenburna värmesystem i byggnader
Utvärdering av energianvändning, minskning av effekttoppar och påverkan på inomhusklimat

Examensarbete inom masterprogrammet Konstruktionsteknik och Byggnadsteknologi

ARVID THEGERSTRÖM

EMIL VENDELSTRAND

Institutionen för Arkitektur och Samhällsbyggnadsteknik
Avdelningen för Installationsteknik
Chalmers tekniska högskola

SAMMANFATTNING

Med det ökande behovet av energieffektivitet i byggsektorn kan mer avancerade reglerstrategier bli viktiga för framtida värmesystem. Arbetet undersöker implementeringen samt effekten av att använda modellprediktiv styrning (MPC) genom att optimera framledningstemperaturen i en modern kontorsbyggnad. Arbetet utvärderar energibesparingar, kapning av effekttoppar samt hur inneklimatet påverkades.

För att utvärdera kontrollstrategin användes en referensbyggnad i det avancerade simuleringsprogrammet IDA ICE. Eftersom mjukvaran inte stödjer modellprediktiv kontroll implementerades en co-simulering mellan IDA ICE och Python. Förenklade resistans-kapacitansmodeller användes för att förutse innetemperaturen i den modellprediktiva kontrollen.

Simuleringarna genomfördes under två veckor för att minimera beräkningstiden och utfördes i mars för att utnyttja värme från solen. Inledningsvis indikerade resultaten en energibesparing på 20–30% när MPC implementerades jämfört med ett traditionellt reglersystem. Efter att effekten från temperaturskillnader eliminerats minskade besparingarna till 3-5%. Effekttopparna kapades med ett genomsnitt på 26% under en vecka medan inomhusklimatet upprätthölls inom de angivna gränserna. Vidare testades styrningen mot felaktiga prognoser för utetemperatur och närvaron i byggnaden. Resultaten indikerade en robust styrning där återkopplingen i den slutna loopen höll innetemperaturen inom de angivna gränserna.

Flera felkällor och begränsningar identifierades. Exempelvis är det inte säkert att resultaten från den förkortade simuleringsperioden på två veckor är tillämpbar på andra delar av uppvärmningssäsongen. Dessutom, genom att enbart fokusera på mars skapas ett ideellt scenario, eftersom förhållandena i mars vanligtvis är gynnsamma för en MPC på grund av ett mindre uppvärmningsbehov och betydande solinstrålning. Bortsett från felkällor och begränsningar visar resultaten tydligt potentialen med modellprediktiv styrning även om ytterligare tester på en fysisk byggnad krävs för att verifiera detta. Slutligen tydliggör arbetet att MPC utgör en intressant väg framåt för att öka energieffektiviteten i moderna byggnader.

Nyckelord: Modellprediktiv styrning (MPC), Co-simulering, IDA ICE, Resistans-kapacitans (RC), Kapning av effekttoppar, Inomhusklimat, Energieffektivisering

Contents

Preface

This Master's thesis, comprising 30 credits, was conducted at the Department of Architecture and Civil Engineering, Division of Building Services Engineering, at Chalmers University of Technology, Sweden. The project was carried out in collaboration with Ingenjörsbyrån Andersson & Hultmark AB.

Throughout the course of this project, numerous individuals have provided valuable insights and support. First and foremost, we would like to express our gratitude to our examiner, Anders Trüschel, and supervisor, Torbjörn Lindholm, for their continuous guidance throughout the thesis work. We would also like to extend our sincere thanks to our supervisors at Andersson & Hultmark, Gustav Thuresson and Staffan Sjöberg, along with the rest of the staff, for their daily guidance and encouragement.

Gothenburg, May 2026
Arvid Thegerström & Emil Vendelstrand

Notations

Greek letters

λ	Thermal conductivity $[W/mK]$
ρ	Density $[kg/m^3]$

Roman upper case letters

AHU	Air handling unit
C	Heat capacity [J/K]
CAV	Constant air volume
COP	Coefficient of performance
NRMSE	Normalized root mean square error
MPC	Model predictive control
Q	Supplied heat [W]
R	Thermal resistance [K/W]
RC	Resistance capacitance
RMSE	Root mean square error
SFP	Specific fan power
T	Temperature [°C]
VAV	Variable air volume

Roman lower case letters

c	Specific heat capacity $[J/kgK]$
k	Current time step
n	Prediction horizon
v	Supply temperature [°C]
w	Weighting factor
y	Indoor temperature [°C]

1 Introduction

The building-sector is undergoing a transition where the clients are increasingly more interested in lowering the environmental impact. During 2022, the building sector accounted for 34 % of Sweden's total energy use where 77% of this usage emerges from heating (Boverket, 2024). In many cases, building envelope components have reached their potential regarding energy efficiency, meaning other solutions to lower the heating energy use must be investigated.

1.1 Background

A building's indoor environment must ensure the health, comfort and operational functionality for the tenants (Petersson, 2014). To fulfill these demands, several different building services are installed including heating, cooling and ventilation. In cold climates, the heating accounts for the majority of the energy usage when a building is in operation. Traditionally, the heating system is controlled by measuring the outside temperature which decides the supply temperature towards the radiators. To further increase the accuracy of the heating system, indoor temperature sensors can be used as feedback to control. Furthermore, recent years have seen an increase in the installation of sensors, able to measure parameters such as temperature, solar radiation, wind, and relative humidity along with forecasts. Integration of these sensors and forecasts enables model-based control of buildings.

Model-based control utilizes a mathematical representation of the building to continuously optimize the supply temperature. By accounting for both real-time measurements and weather forecasts, the system can proactively predict the building's thermal behavior and adjust the heating accordingly. This technology is implemented in several buildings in Sweden and there is extensive research in the field today. The latest development by industry-leading designers provides model predictive control (MPC) combined with the use of artificial intelligence (AI) to further optimize the control system.

1.2 Aim and purpose

The primary objective of this thesis was to evaluate the implementation and performance of MPC in modern hydronic heating systems. To achieve this, the study first conducted a literature review to identify energy savings achieved as of today. Furthermore, the research assesses to what extent a building can be modeled to match on-site measurements. The final purpose is to quantify the operational benefits of an MPC in a modern building context, focusing on its ability to optimize thermal comfort while reducing energy use.

1.3 Limitations

Due to the size of the reference building, the control scheme was implemented only in selected zones, as detailed in Chapter 5. To optimize computational efficiency, the simulation and analysis were restricted to a two-week period during the heating season. This duration was deemed sufficient to fulfill the study's objectives and evaluate the controller's performance.

Finally, economic implications of the system were not considered in depth, as the research primarily prioritized the technical aspect of implementing model predictive control.

1.4 Research questions

The research questions are stated below, based on the aim and purpose of the thesis.

- To what extent can model predictive control reduce energy use in a high-complexity office building compared to a traditional control system?
- How effective is model predictive control in performing peak power shaving?
- How is the thermal comfort affected by the model predictive control's supply temperatures and can the system maintain temperature stability within defined comfort boundaries?

1.5 Social, ethical and ecological aspects

Societal aspects have been identified as the effect on indoor environment, regarding the comfort of the tenants. The thesis will not consider the ethical or ecological aspects of implementing the technology since it was deemed irrelevant to the scope of the thesis.

1.6 Use of artificial intelligence

Artificial intelligence has been used as an aid in developing and debugging the programming code required to execute the simulation. It has also been used as a tool to enhance sentence structure and correct grammatical errors throughout the text. AI has not been used as a source for research.

2 Method

The thesis consists of a literature study on how modern control systems are implemented in today's buildings, answering how they operate, on what input parameters and what effect it has yielded. The literature study also focused on obstacles in implementing modern control systems. The desired information was retrieved from consultation with industry experts, interviews with companies providing modern control systems as well as scientific literature.

The second phase of the thesis focused on implementing a model predictive control system. A reference building already modeled in IDA ICE was provided by Andersson & Hultmark, where data from on-site measurements was available regarding heating, cooling and electricity. The measured data was used to adjust the model to resemble reality.

Once the adjustments were complete, the advanced building model in IDA ICE was set up in a co-simulation environment, where a custom-designed MPC developed in Python was implemented. By utilizing IDA ICE to represent the building and Python for the control algorithms, the building's thermal behavior was accurately modeled. The simulation method aimed to replicate real-world operations. The performance of the MPC was evaluated and compared to a traditional control system. The robustness of the MPC was examined by introducing forecast uncertainties regarding temperature and occupancy.

2.1 Simulation method

The simulation process consisted of three main steps, namely acquire training data, build zone models and execute the co-simulation.

2.1.1 Acquire training data

Initially, an appropriate set of training data was acquired using the reference model in IDA ICE, see Figure 2.1.

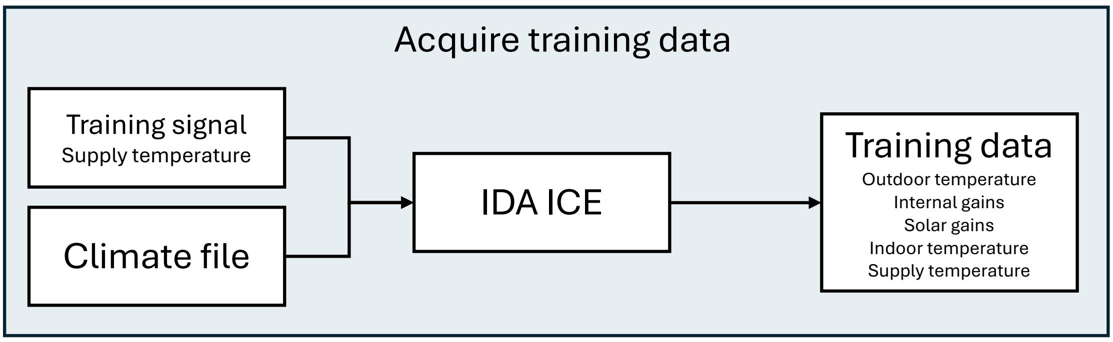

Figure 2.1: Workflow chart for acquiring training data from reference building in IDA ICE.

A random training signal with varying supply temperature was created and together with the climate file from IDA ICE a simulation was executed. The random supply temperature created fluctuations in the indoor temperature which enabled the extracted training data to capture the building dynamics.

2.1.2 Build zone models

The next step in the simulation process was to build the mathematical zone models required by the model predictive controller, see Figure 2.2.

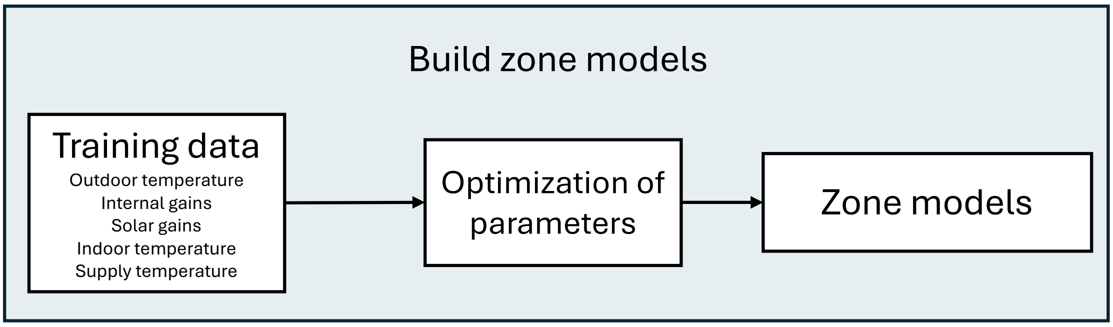

Figure 2.2: Workflow for creating zone models for based on training data extracted from IDA ICE.

Using the previously obtained training data, the physical building parameters for each zone were optimized to ensure that the zone models accurately replicated the behavior in IDA ICE. These models were used to predict the future indoor temperatures.

2.1.3 Co-simulation

The final step of the simulation process was to set up the co-simulation between IDA ICE and the MPC, see Figure 2.3.

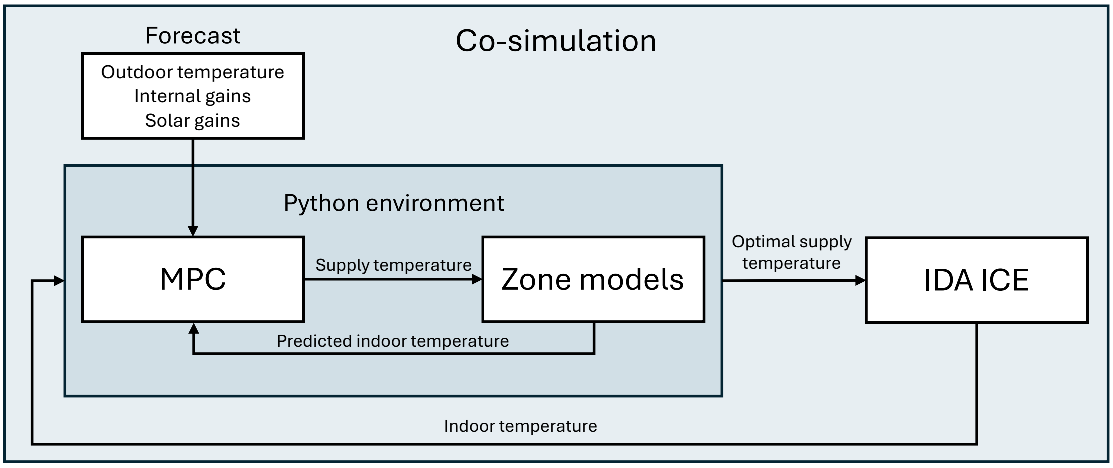

Figure 2.3: Workflow for co-simulation between the MPC and IDA ICE.

This control strategy was not supported by the software, hence a co-simulation with Python was implemented. The forecast for outdoor temperature, internal gains and solar gains was exported into the MPC together with the indoor temperature from IDA ICE to provide feedback. Based on the imported data, the MPC iteratively proposes different control signals for the supply temperature and the zone models calculates a predicted indoor temperature. After enough iterations, the optimal supply temperature is sent to IDA ICE, creating the desired simulation loop. The process is repeated every 15 minutes.

2.1.4 Summarized simulation method

The summarized simulation method is presented in Figure 2.4.

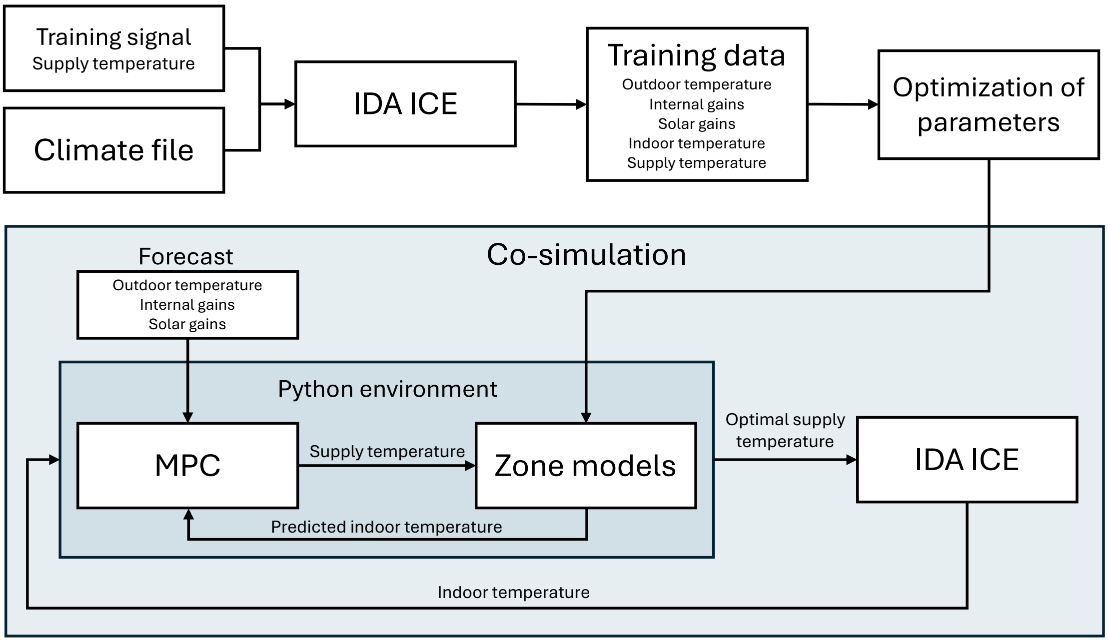

Figure 2.4: Overview of the entire simulation method connecting all three previous steps.

As Figure 2.4 displays, the simulation procedure is initiated with collecting training data that is used for the optimization of building parameters. With the acquired zone models the co-simulation loop is completed and the final simulation can begin.

3 Literature study

This chapter provides the theoretical and contextual foundation for the thesis by reviewing the current state of knowledge regarding implementation of MPC in buildings. The literature study is structured into two primary sections to capture both the academic and industrial perspectives. First, a compilation of different studies that examines energy savings when implementing MPC was examined. Secondly, an investigation of commercially available MPC solutions in Sweden was carried out.

3.1 Research study

In a licentiate essay by Olsson (2014), the possible energy savings utilizing forecast-based control is compared to feedforward, feedback and model-based control. The essay is based upon simulations in IDA ICE 4.6 and the results indicate that model-based control with predicted weather saves 10 kWh/m^2 in comparison with feedforward control. Although, the conclusion from the results states the largest energy saving potential lies in adjusting supply temperature to current heating demand, meaning the weather forecast has small impact on energy usage compared to real-time model-based control.

To verify the results of the thesis, nine similar studies results were compared whom published between 2010 and 2024. All nine studies have been found from the research of Khabbazi et al. (2025) and represents real-world applications. In 2010, a study by Z. Liao (2010) evaluated the energy savings for a commercial building with radiators when applying MPC to the supply temperature and the resulting energy savings varied between 9 and 32.1%. In a study by Prívara et al. (2011), a commercial building with built-in heating system in a concrete ceiling was evaluated with MPC for the supply temperature. The MPC achieved energy savings of 29% (Prívara et al., 2011).

A real-world application where the supply temperature was controlled with an MPC, savings between 15% and 28% was recorded when compared to heating curve control (Široký et al., 2011). Although, the experiment was carried out with equivalent, but not equal conditions. Therefore the research utilized normalization of savings based on the outdoor temperature. The researchers points out two issues in applying MPC to a building, firstly all buildings are unique and savings will vary. Secondly, the cost of installing the technology, including the time-consuming part of modeling, must be considered (Široký et al., 2011).

An approach where the supply temperature and ventilation air flow was controlled by MPC was examined for a basement located in Stockholm in a research paper by Parisio et al. (2014). The findings discovered energy savings between 31 and 33% (Parisio et al., 2014). A study in Switzerland applied MPC to an office building of 2700 m^2 which reported savings of 31.9% (Lindelöf et al., 2018). A study for a large office building in Hamburg utilized an MPC controller for the supply temperature which resulted in 30% reduction for the energy use compared to a feedforward control system (Svenne Freund, 2021). A commercial building in Brussels with MPC controller for the supply temperature managed to reduce the energy use by 11.7% (Sampaio et al., 2021). A study by Stoffel et al. (2024) presented savings between 5.3 and 22.2% when comparing MPC to PID controllers for heating, cooling and ventilation. A Norwegian office building managed to minimize its energy use by 10% when MPC was applied to the supply temperature and compared to rule-based control with thermostats (Lolli et al., 2024).

Results from the research study are compiled in Figure 3.1.

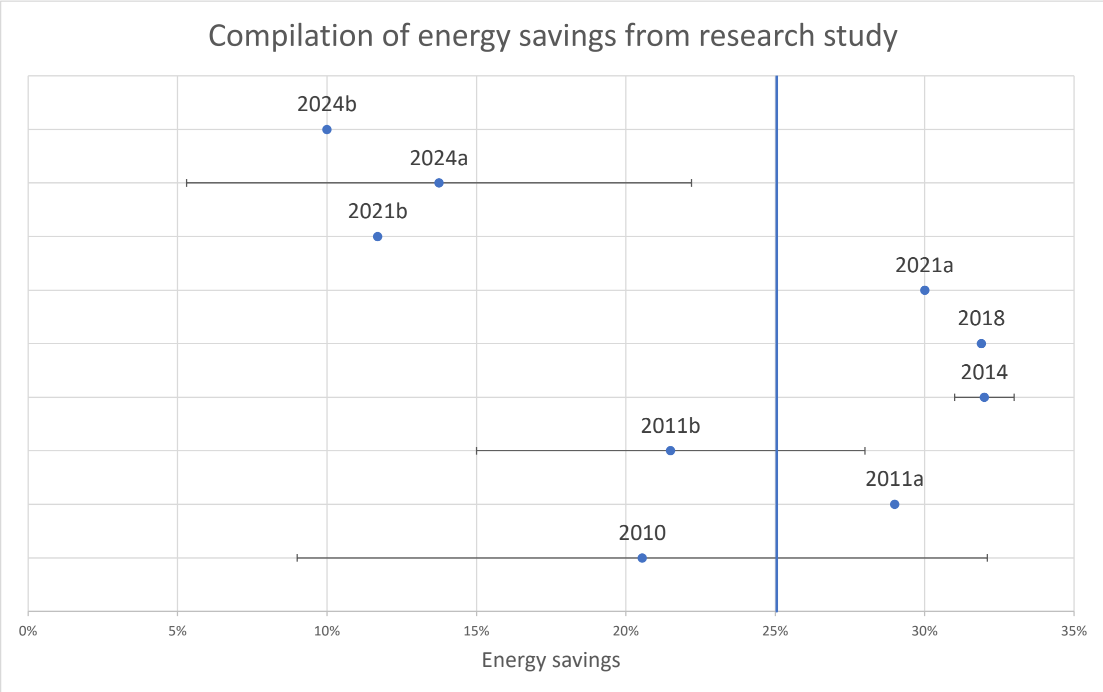

Figure 3.1: Compilation of results from research study where percentage of energy saved is displayed. The blue line denotes the average savings from all studies.

While MPC is a tool which provides the most optimal solution, the model-based format is bound to cause differences between the simulated and actual performance of the building. According to X. Ding (2025), the differences emerge from obligatory simplifications when modeling to maintain the computational speed. X. Ding (2025) exemplifies by stating that the physics of the building along with the cost function applied to the MPC are usually simplified by approximations. X. Ding (2025) continues stating challenges with modeling buildings, where the complexity in dynamics and unpredictability in occupant behavior causes difficulties.

3.2 Available products

There are multiple products on the market today that offers smart control in different ways. Most products uses some sort of AI model to control the system by reading data from sensors and learning the behavior of the occupants.

The municipality of Gothenburg, Göteborgs stad, has invested in services which provides MPC in buildings (P. Valo, personal communication, 2026). Two services has been implemented, namely Algeno and Myrspoven. Algeno is a company which provides a mathematical model whom updates regularly, based on previous data and AI (Algeno AB, 2024). The mathematical model operates at a time horizon of 48 hours and considers forecasts for weather and internal gains. The MPC is programmed to optimize for energy performance, energy prices and power peaks (Algeno AB, 2024). According to P. Valo (personal communication, 2026), the co-operation with Algeno has saved on average 7% heating energy since installation and few complaints from occupants has emerged.

Myrspoven is a company which offers similar services as Algeno but applies MPC to heating cooling and ventilation. However, in Göteborgs stad's pilot projects only heating and ventilation was applied (P. Valo, personal communication, 2026). The service utilizes machine learning to comprehend the dynamics of the building and the optimization is carried out every 15 minutes (Myrspoven, n.d.). The reported savings for Göteborgs stad was 11% (P. Valo, personal communication, 2026).

4 Theory

A building is composed of numerous complex and interacting systems that together define its performance and efficiency. To optimize these systems it is fundamental to first understand the underlying physical mechanisms that govern the indoor thermal climate. The indoor environment is a dynamic result of the continuous energy exchange between the building's envelope, its internal heat gains, and the outdoor climate. By identifying the key variables that influence these thermal processes, such as insulation levels and thermal mass, strategies for predictive control can be effectively implemented to manage energy use without compromising occupant comfort. The following sections aims to explain the basic functions of a building.

4.1 Heat balance

Heat balance is achieved when the heat gains inside the building equals the heat losses from the building. When describing the heat balance of a building, four main sources of heat fluxes can be found (Al-Sanea et al., 2017). These are:

1. Direct heat gain from solar radiation
2. Transmission losses from building envelope
3. Internal gains from indoor activity
4. Air leakages through ventilation and infiltration

In order to obtain comfortable indoor climate, technical systems can add or remove heat to adjust the heat balance and maintain a constant indoor temperature. More about these technical systems in 4.5.

4.2 Peak power demand

Power is a measure of the amount of energy a device consumes at a specific moment, typically expressed in kilowatts (kW). This is not to be confused with energy, which is a measure describing the amount of power used over a specific period of time, typically expressed in kilowatt-hours (kWh). Peak power demand occurs when energy usage reaches its highest level at a specific moment, usually when a lot of electrical devices are used at the same time (Göteborg Energi, n.d.). This creates high pressure on the power grid. However, by distributing the usage more evenly and effectively reducing peak power demand, the overall strain on the power grid can be reduced.

Occupant behavior is a crucial factor in reducing peak power demand. By distributing power demanding activities in the household over a longer period of time, the peak demand can be reduced. Another way of reducing peak demand is by controlling the heating system in a smart way by minimizing usage at the hours of the day where the highest peaks are. At night, the energy price is often lower than during the day making energy usage beneficial during these hours. For example, the thermal inertia can be utilized to pre-heat the building during the night resulting in a more evenly distributed energy use and lower peak demands.

4.3 Thermal inertia

Thermal inertia is defined as a material's resistance to temperature changes (Al-Sanea et al., 2017). It can be described as how the building's structure acts as a thermal buffer. Heavy constructions, for example houses built of heavy-weight material such as concrete, stone or bricks, generally have a large thermal inertia. Light constructions, such as timber or steel frames, often exhibits a lower thermal inertia. The ability to shift and shave peak demands increases with larger thermal mass of the building . To reduce the energy demand of buildings in heating dominating climates, increasing the thermal resistance of the building envelope is generally seen as the most crucial factor. Depending on the temperature difference with the surroundings, the thermal mass of a building can either absorb, store or release heat. The amount of heat stored is determined by the material's density (ρ) and the specific heat capacity (c_p) while the rate of heat exchange depends on the thermal conductivity (λ).

Thermal inertia can have different effects on buildings depending on season, temperature fluctuations and building design (Al-Sanea et al., 2017). During summer, the thermal inertia of a building can help reduce overheating risks and excessive cooling loads. In intermediate seasons, during spring and autumn, thermal inertia can instead help with creating a sufficient indoor climate without the need of active cooling and heating, generating a passive temperature control.

However, larger thermal mass does not always imply better indoor environment. Buildings characterized by high thermal mass exhibit a slower thermal response, requiring more time to reach heating or cooling setpoints. This can lead to temporary thermal discomfort for occupants if not managed correctly. Furthermore, the longer preheating or pre-cooling periods necessary to charge the building's structure may result in increased energy consumption if the control strategy is not optimized for the building's specific inertia (Al-Sanea et al., 2017).

The findings of Al-Sanea et al. (2017) literature overview about the impact of thermal inertia in buildings show different opinions. The magnitude of savings achieved through increased thermal inertia in buildings also varies significantly. Some study's conclude that the level of thermal inertia has a negligible influence on heating energy demand. However, most studies do find that thermal inertia have a positive effect on both cooling and heating demands.

4.4 Modeling a building

There are several different approaches to model a zone in a building. This thesis utilizes the analogy of modeling buildings as circuits, namely resistance capacitance models. The resistance in an arbitrary building element is visualized in Figure 4.1.

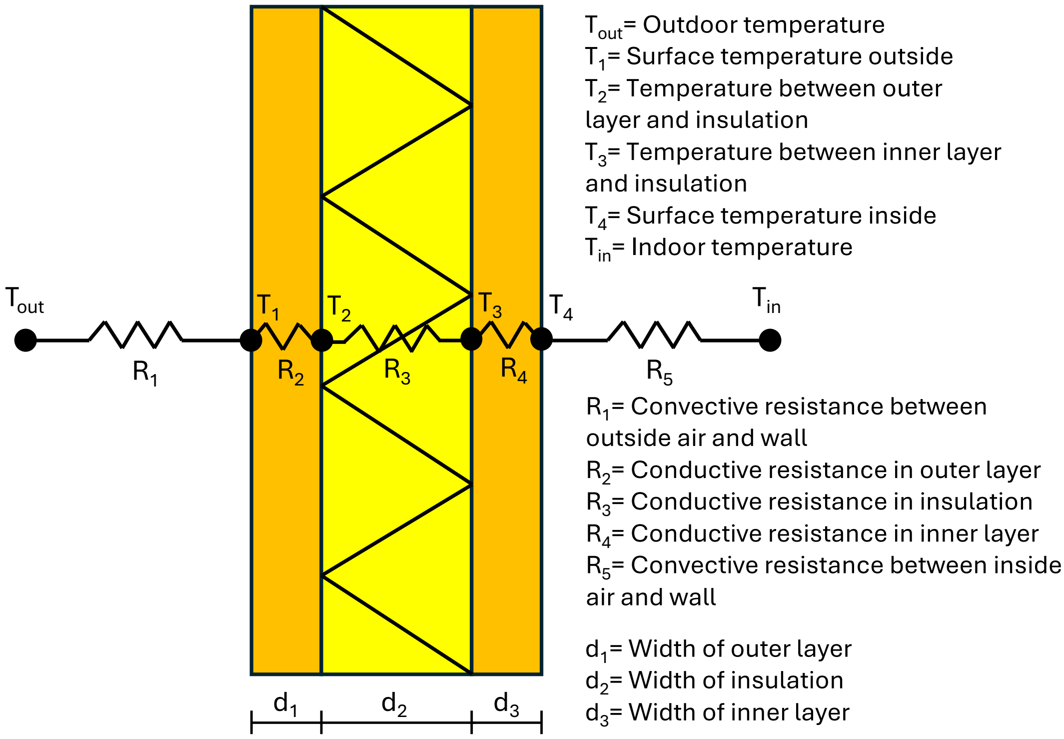

Figure 4.1: Heat transfer through a single building element where the resistances has the unit K/W and the temperatures °C

As seen in Figure 4.1, both the convective and conductive heat transfer in the building element is considered. Every resistance describes the amount of heat exchange between the temperatures. The conductive resistances R_{2-4} are calculated according to Equation (4.1), the convective resistances R_1 and R_5 are calculated according to Equation (4.2) and the resulting heat exchange is calculated according to Equation (4.3).

$$R_n = 1/\frac{\lambda_n}{d_{n-1}}A \tag{4.1}$$

$$R_n = 1/h_n A \tag{4.2}$$

$$Q_{tot} = \frac{T_{in} - T_{out}}{R_1 + R_2 + R_3 + R_4 + R_5}[W] \tag{4.3}$$

Where λ_n is the thermal conductivity of material n with the unit W/mK and h_n denotes the convective heat transfer coefficient between the building material and air with the unit W/m^2K.

To further develop the model, the building material's capacity to store heat is considered. This is modeled by assuming all temperature nodes has heat storage capacity and is presented in Figure 4.2.

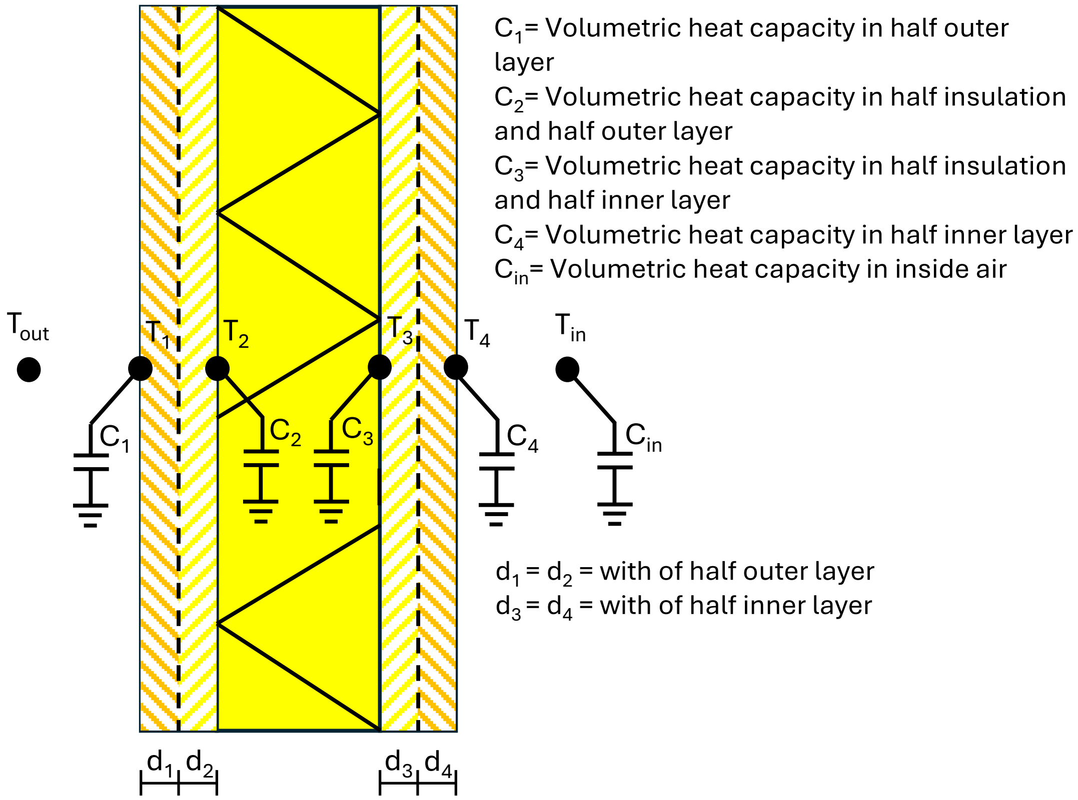

Figure 4.2: Volumetric heat capacity in a single building element.

Figure 4.2 displays a simplified approach to decide what sections stores heat to what temperature nodes. The heat storage capacity has the unit J/K and is calculated according to Equation (4.4)

$$C_n = d_n \rho_n c_{p,n} A [J/K] \tag{4.4}$$

If the theory from Figure 4.1 and 4.2 are used as one circuit the result is according to Figure 4.3.

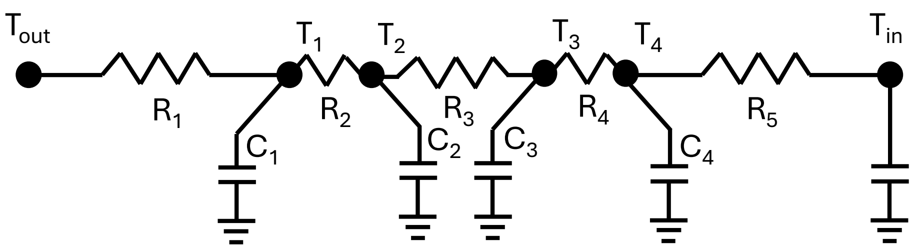

Figure 4.3: Resulting circuit from previous theory involving heat transfer and volumetric heat capacity.

The different temperature nodes can be described with the differential equations stated in (4.5)-(4.7).

$$C_1\frac{dT_1}{dt} = \frac{T_{out} - T_1}{R_1} \tag{4.5}$$

$$C_n\frac{dT_n}{dt} = \frac{T_{n+1} - T_n}{R_{n+1}} + \frac{T_{n-1} - T_n}{R_n} \tag{4.6}$$

$$C_{in}\frac{dT_{in}}{dt} = \frac{T_4 - T_{in}}{R_5} \tag{4.7}$$

With the derived equations the model can be expanded to represent an entire zone in a building. An example of this is displayed in Figure 4.4.

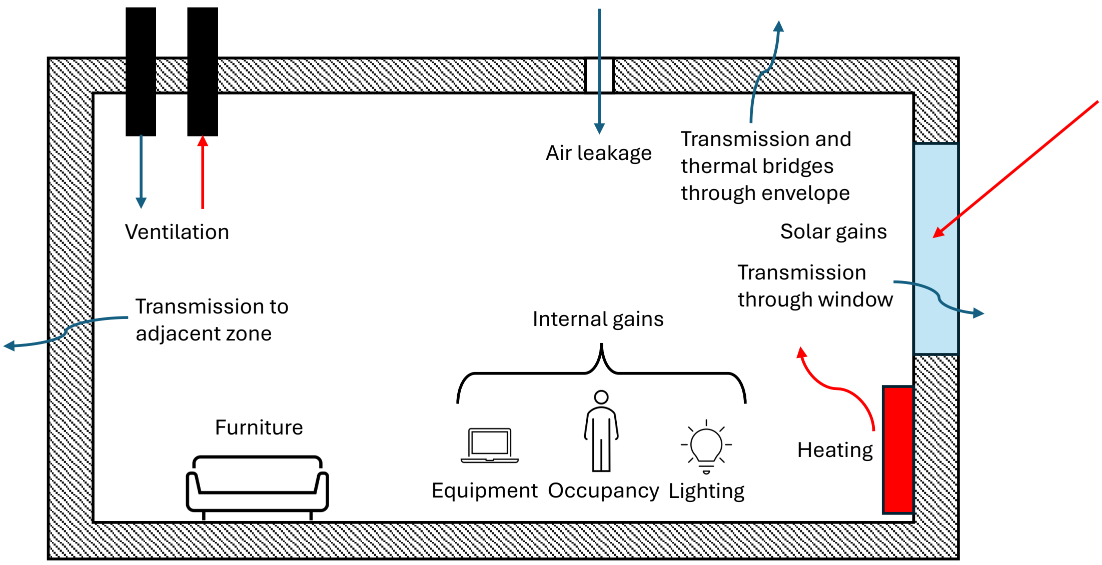

Figure 4.4: Example of gains and losses for one zone, modeled according to IDA ICE schematic.

Figure 4.4 considers the gains and losses from ventilation, thermal bridges and transmission to the outside and adjacent zones through walls and windows. It also considers air leakage, internal gains from equipment, occupancy and lighting, heating from radiators along with thermal storage capacity of the furniture in the zone. By adding together the theory explained in the chapter the circuit in Figure 4.5 is achieved.

Figure 4.5: Circuit for one zone in a building

Figure 4.5 adopts the following notation:

- T denotes temperature [°C].
- R denotes thermal resistance [K/W].
- Q denotes supplied thermal power [W].
- C denotes heat capacity [J/K].

The equations employ the following indeces:

- out denotes outdoor.
- in denotes indoor.
- ex denotes external walls.
- r denotes roof.
- rad denotes radiators.
- int denotes internal walls.
- f denotes floors.
- win denotes windows.

- $furn$ denotes furniture.
- $solar$ denotes solar heat gains.
- $leak$ denotes infiltration/air leakage.
- $vent$ denotes ventilation.
- $int.gains$ denotes internal heat gains.
- adj denotes adjacent zones.

The resulting differential equations will not be presented but are derived with the same procedure as for Figure 4.3.

Figure 4.5 is a detailed model with few assumptions. Normally, this type of modeling is simplified by lumping the model. A lumped model means to merge the volumetric heat capacity in a zone for all layers on the inside of the insulation. The lumped model is further explained in section 5.3.3.

4.5 Control systems

A building's indoor environment must ensure the health, comfort and operational functionality for the tenants (Petersson, 2014). To fulfill these demands, several different building services are installed including heating, cooling and ventilation. Regarding heating systems, the control is based on different procedures. Namely feedforward, feedback or model-based control.

4.5.1 Feedforward control

Feedforward control for radiators is based on the supply temperature curve, which is individually adjusted for each building. The hydronic heating system operates according to a graph plotting the supply temperature in the system against the outside temperature, see Figure 4.6.

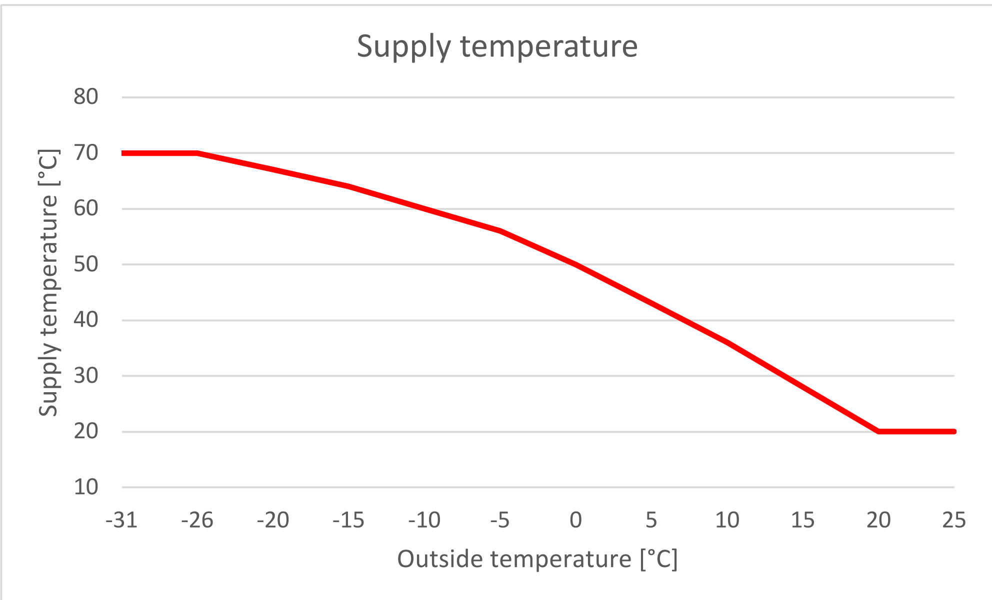

Figure 4.6: Example of standard supply temperature curve with a maximum temperature of 70°C

4.5.2 Feedback control

Even though feedforward control has proven to be an efficient and simple control, it does not consider the effects from activity inside the building. A feedback control simply adds the indoor temperature to the control system which accounts for internal gains and losses. In feedback controls' simplest form a P-control is utilized, meaning adding thermostats to each radiator for local control with a P-band. The P-band is displayed in Figure 4.7.

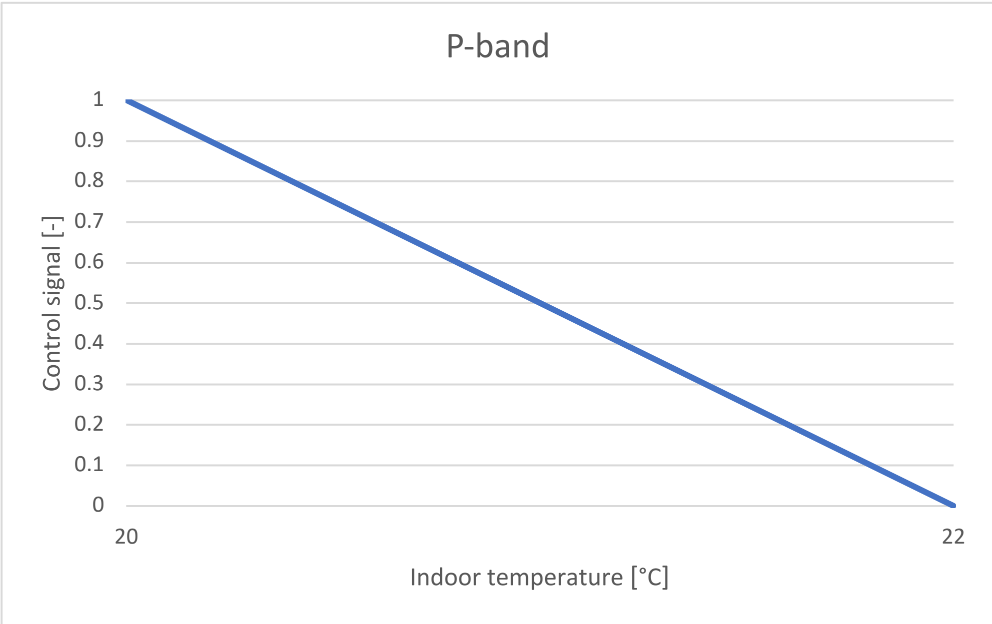

Figure 4.7: Example of a 2°C P-band with a setpoint of 22°C.

As displayed in Figure 4.7 the control signal is decided by the indoor temperature. If the temperature falls below 20 °C, the valve is fully open and closes linearly as the temperature increases to 22 °C when it becomes fully shut.

4.5.3 Model predictive control

Model predictive control utilizes the ability to predict future indoor temperature by considering weather forecasts and behavior of the building such as thermal inertia. This makes it possible to calculate the most efficient way to maintain the indoor temperature within defined boundaries. The basic terms for MPC consists of predicted output (predicted temperature), reference output (reference temperature), prediction horizon, control input (supply temperature) and control horizon. A graph showing the presented terms is viewable in Figure 4.8.

As Figure 4.8 illustrates, the supply temperature aims to align the predicted temperature with the reference temperature in the most effective control sequence. When designing the MPC, the prediction horizon can be altered which changes the time horizon the MPC calculates the state of the building. The control horizon operates with the same principle as the prediction horizon but instead decides the amount of time steps ahead the MPC proposes a control scheme and is usually in a shorter time span for faster computing.

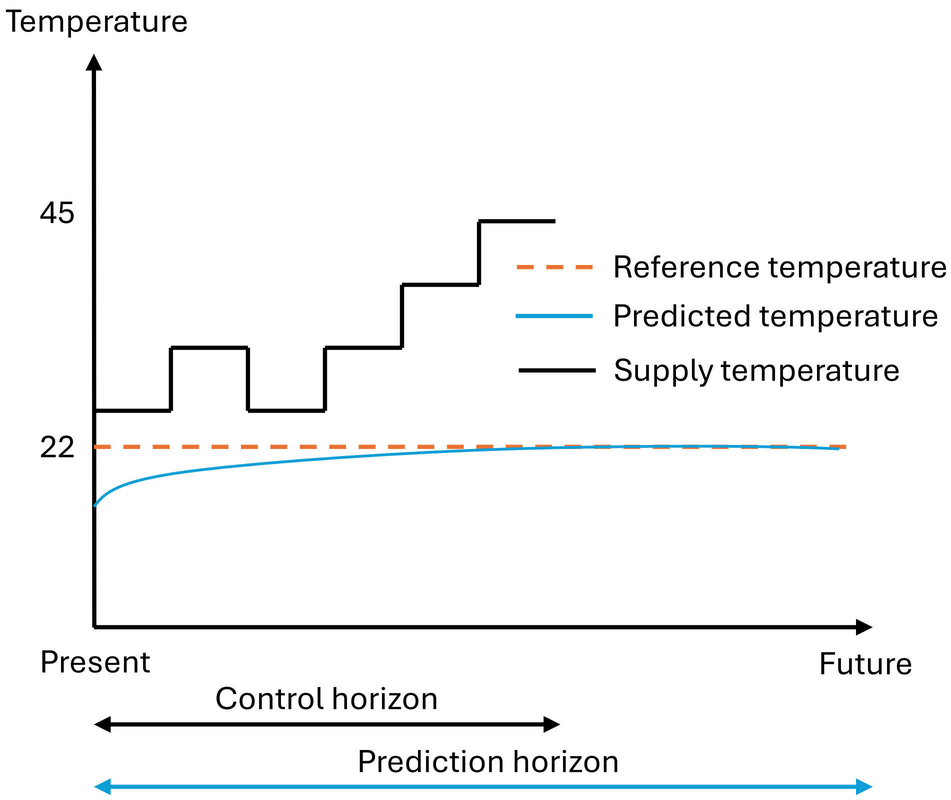

Figure 4.8: An MPC graph plotting temperature against time with the defined terms, inspired by figure from Mathworks (n.d.-b).

When designing an MPC, the aim is to achieve the most effective control scheme by minimizing a cost function that balances multiple objectives. In building climate application, this typically involves trade-off between thermal comfort and energy savings. Formally, the objective function J is formulated as a weighted sum of linear and quadratic terms according to Equation (4.8) (Mathworks, n.d.-b).

$$J = \sum_{k=1}^{n} \left(w_y |y_k - y_{ref}| + w_v \cdot v_k + w_{\Delta v} \cdot (\Delta v_k)^2 + w_s \cdot \epsilon_k \right) \tag{4.8}$$

Where:

- k denotes the current time step and n the prediction horizon.
- ref is the temperature setpoint.
- y is the indoor temperature.
- v is the supply temperature.
- $\Delta v = v_k - v_{k-1}$ represents the change in supply temperature between steps.
- ϵ is a variable representing the comfort boundary violation.
- $w_y, w_v, w_{\Delta v}, w_s$ are weighting factors set by the designer to prioritize different objectives.

The cost function consists of four different terms, each addressing a specific objective. The first weighting factor, w_y, penalizes temperature deviations from the reference temperature with a linear cost. The second factor, w_v, focuses on energy cost by pressuring the boiler to a lower supply temperature. The third factor, $w_{\Delta v}$, is a quadratic cost that penalizes large, sudden jumps in supply temperature to reduce peak power demand. The term is quadratic to penalize large rapid changes but allows minor changes. The last weighting factor, w_s, penalizes the ϵ variable to ensure that the solver stays within the indoor temperature boundaries. These weights can be adjusted in different ways to prioritize different objectives. There are also constraints on y_k and u_k, where y_k is constrained between defined indoor comfort boundaries and u_k is constrained between set temperature for the boiler according to building specifications. The weights and constraints utilized in this thesis is thoroughly described in section 6.3.1.

Since the objective of the MPC is to optimize the supply temperature, it must be able to calculate future temperature in the building. This is usually done by developing state-space models. A state-space model is a formulation which utilizes first-order differential equations to describe and predict future states of a model (Mathworks, n.d.-a). The formulation utilized in this thesis is according to Equation (4.9) and (4.10). Equation 4.9 contains the zone model and calculates the future states of the building. Equation (4.10) extracts the desired state, in this case the indoor temperature.

$$\dot{x}(t) = Ax(t) + Bu(t) + Ev(t) \tag{4.9}$$

$$y(t) = Cx(t) + Du(t) \tag{4.10}$$

- $\dot{x}(t)$: The state derivative, representing the rate of change of the temperatures in the system.
- $x(t)$: The state vector, containing the internal temperatures of the model.
- $u(t)$: A vector containing the disturbances such as climate and activity inside the building
- $v(t)$: The control input vector, in this case, the supply temperature from the boiler.
- A : The system matrix, describing the heat transfer between states based on thermal resistance (R) and heat capacity (C).
- B : The disturbance input matrix, describing how disturbances affect the different states.
- E : The control input matrix, describing how the controlled supply temperature affects the system.
- $y(t)$: The output vector, representing the indoor temperature.
- C - The output matrix, used to extract a specific state. Contains ones and zeros.
- D - The feedthrough matrix, representing any direct coupling between inputs and outputs (usually zero in building models).

5 Modeling

This chapter explains the conditions and systems in the reference building, how it was altered to minimize the gap with measured field values and how the models were converted from IDA ICE to mathematical state-space equations. The chapter also describes how the MPC was implemented into the building along with a description of how forecast uncertainty was analyzed.

5.1 Reference building

The building consists of 12 floors, see Figure 5.1, where the first floor is used for restaurant, the second floor is a library, the nine floors above for offices and a basement with bicycle garage, control room and air handling units (AHU). On the roof of the building a technical room with an air handling unit is installed. On two facades of the building a glass facade is constructed creating a terrace. The temperature on the terrace is controlled with ventilation hatches with the purpose to maintain a temperature below 25 °C.

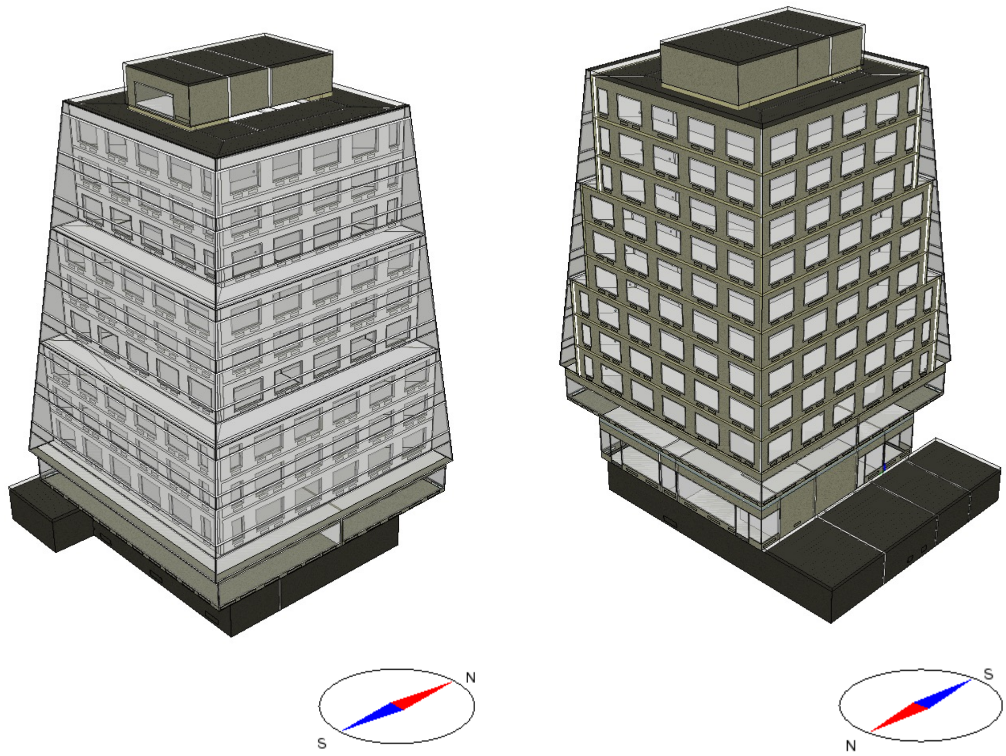

Figure 5.1: The reference building used in this thesis in two directions.

The evaluated building is mainly heated with radiators. These are placed along the perimeter of the building beneath the windows. The radiators are equipped with local P-controllers with an assumed P-band of 1.5°C and a setpoint of 22°C. Heat is supplied to the building using ground source heating and the heating circuit's maximum temperature difference is 45/30°C.

The building has active cooling via the ventilation system. The building's ventilation system is of type VAV with temperature and CO_2 control. If the temperature rises above 23 °C or the CO_2 concentration exceeds 1100 PPM the airflow is increased with a PI-controller. If the temperature or CO_2 level remains above the setpoint after maximum airflow is reached, the supply air temperature decreases linearly from 18 to 14 °C until setpoints are satisfied.

5.2 IDA ICE model

The building's geometry in IDA ICE was modeled according to the ASHRAE standard 90.1 (ASHRAE, 2022) utilizing perimeter zones according to Figure 5.2.

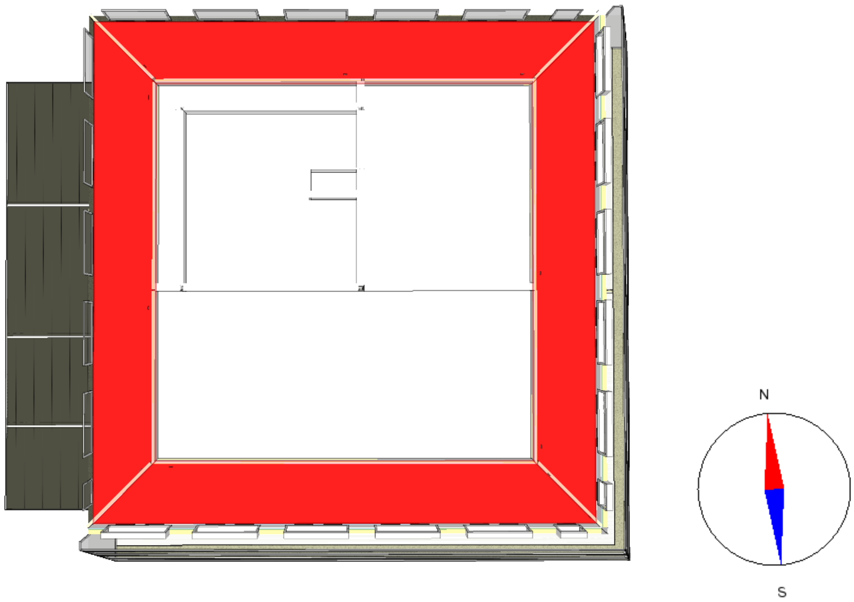

Figure 5.2: Perimeter zones on an arbitrary floor in the building marked in red.

Figure 5.2 displays the perimeter zones in red and a similar modeling is done on all floors with offices. This modeling strategy makes sure the effects from ambient factors that depend on direction, such as solar gains and wind, is not over- or underrated. The sun heats up the southern facade during the day and might result in a cooling need but the northern facade who is mostly affected by the outside temperature has a heating need at the same time. If the entire floor was lumped into one zone this effect would not be considered which generates less trustworthy simulation results. With the perimeter zones the heat flow to the core of the building is limited by the internal walls which was corrected by adding leaks.

To achieve a more realistic simulation, radiators was placed and dimensioned according to drawings. The radiators supply heat based on the supply temperature as well as the water mass flow. The supplied heat is expressed as a non-linear function of the indoor temperature. The maximum supply temperature was as earlier stated 45°C, hence the supply temperature curve was assumed according to Figure 5.3.

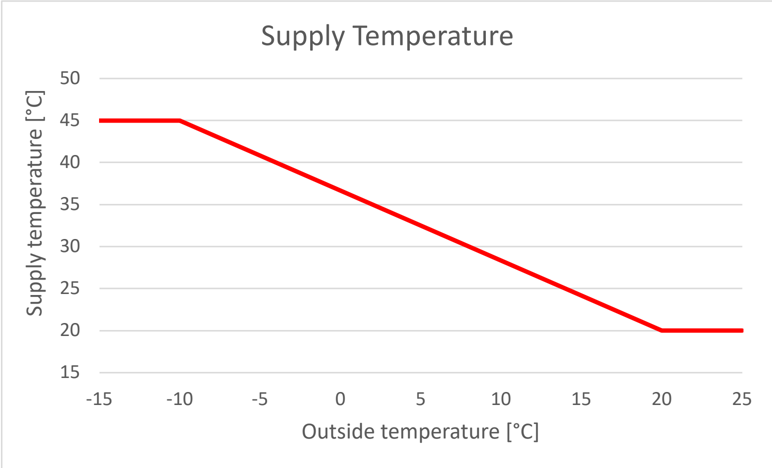

Figure 5.3: Assumed supply temperature curve used in IDA ICE with a maximum of 45°C.

The terraces are controlled by ventilation hatches whom open when the temperature inside exceeds 25°C. Implementing this control sequence into IDA ICE is a heavy simulation measure. To avoid increasing the simulation time, ideal coolers were added on the terraces to maintain the temperature below the setpoint.

The ventilation's control scheme interpreted in IDA ICE is presented Figure 5.4.

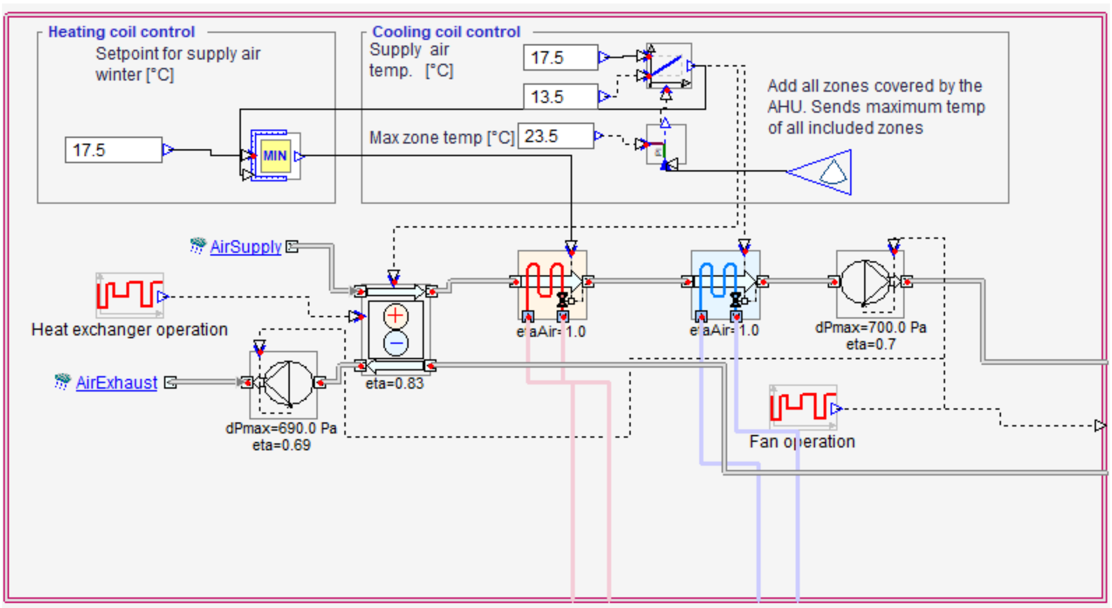

Figure 5.4: Control scheme of air handling unit in IDA ICE

The air handling unit shown in Figure 5.4 consists of supply and return fans, heat exchanger, heating coil and cooling coil. The fans operate at a specific fan power (SFP) of 1.7 $kW/(m^3/s)$ and the heat exchanger has an efficiency of 83%. The temperature rise in the fans is assumed to 0.5°C and the ventilation in the office is active between 6-18 on weekdays, 11-17 on Saturdays and deactivated on Sundays and holidays. The ventilation normally operates at a supply temperature of 18°C but if the temperature rises above the cooling setpoint it decreases to 14°C.

5.2.1 On-site measurements

To create a building model which correlates to reality, on-site measurements were used. The measurements included accumulated energy for heating, cooling, facility electricity and tenant electricity. The verification of the resulting adaption is presented in section 6.1.

For the on-site measurements, the heating energy was measured in the sub-central for the radiators as well as in the air handling units' heaters. The cooling was measured in the AHU coolers. The facility electricity measurement utilized in the thesis to verify the IDA ICE model consisted of the fan operation. However, the fan electricity measurements where lumped in the sub-centrals together with electric radiators in the basement, an elevator and some minor pumps. Assumptions to isolate the ventilation electricity are further described in section 6.1.

The measured values for tenant electricity are presented in Figure 5.5. The on-site measurements were evaluated to create schedules for the occupants, the equipment and the lighting in the IDA ICE model.

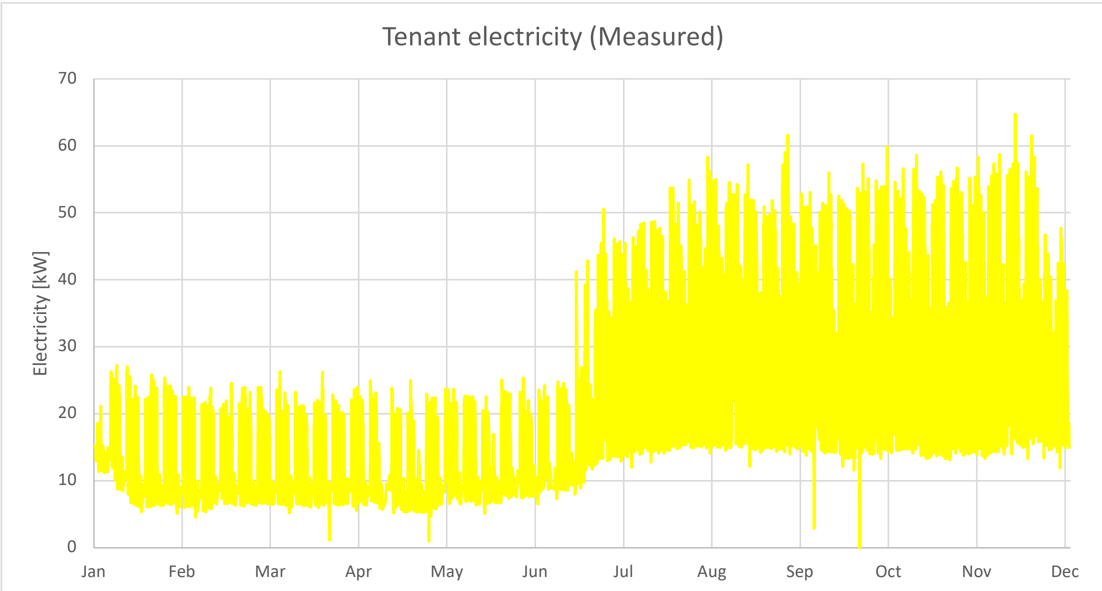

Figure 5.5: Tenant electricity in kW measured on-site during 2025.

Figure 5.5 appears to repeat regularly throughout two periods. From January to the end of June the electricity peaks between 22 and 26 kW every week and for the remainder of the year it was increased to reach peaks above 60 kW as well as behaving more irregularly. The reason for the difference throughout the year is the cause of a restaurant opening on the bottom floor. The conclusion for this thesis is that the first half of the year will be used to create the schedule in IDA ICE since the aim is to investigate only the office spaces in the building. This will be explained more thoroughly in section 5.4. The resulting schedule is according to Figure 5.6.

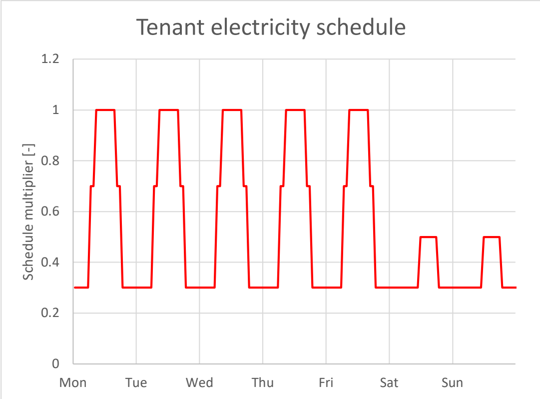

(a) Schedule for tenant electricity in IDA ICE, including lighting and equipment.

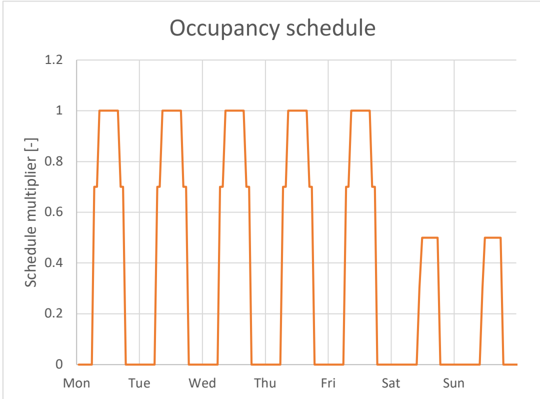

(b) Schedule for occupancy behavior in the building applied in IDA ICE.

Figure 5.6: Schedules used in IDA ICE applied on the office areas, evaluated from measured tenant electricity.

To evaluate the effectiveness of the applied schedule, a graph plotting the tenant electricity during two weeks was created, presented in figure 5.7.

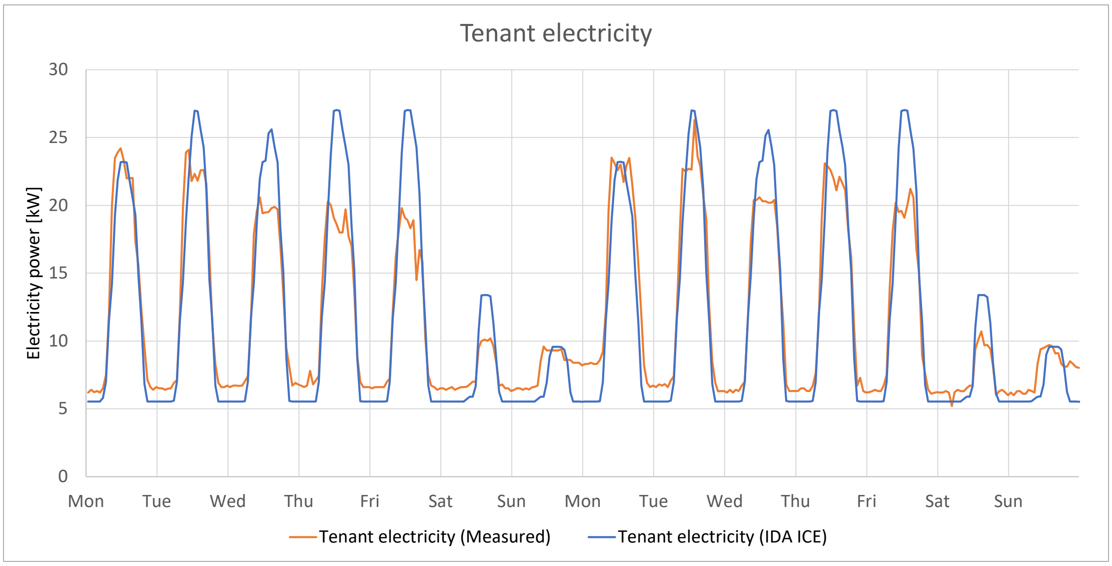

Figure 5.7: Tenant electricity in the building during two weeks in March 2025, expressed in kW. The orange line displays the on-site measurements and the blue line shows the results from simulation.

The schedule appears to have created a reasonable fit to the on-site measurements and has replicated the behavior of the tenants. Although, differences are apparent since the simulation model overestimates peaks and underestimates the valleys.

Although the main part of the building contains open landscape offices, there are some deviations which required a separate schedule such as the stairways, cafe, technical rooms and meeting rooms. A detailed input data report of the IDA ICE model is presented in appendix A.

5.3 Mathematical model

As mentioned in chapter 4, to control a building with MPC the building model needs to be formulated as a state-space model. There are three different approaches to obtain these formulations. Namely white-box, black-box and grey-box models.

5.3.1 White-box model

White-box models considers physics and is created with equations explaining the heat flow in the zone. An example of a white-box model is IDA ICE which estimates the real-world behavior of a building well, but suffers in computational speed. Another example is a detailed circuit according to Figure 4.5. The circuit is an example of a zone in the considered building. The circuit takes into consideration the convection and conduction for outside wall and roof as well as the floor below and adjacent zones. The model also considers the thermal inertia of the radiators and furniture in the room. The drawback with a white-box model is that it requires a lot of input data which is time consuming.

5.3.2 Black-box model

The second option to build a state-space model involves black-box modeling. This method utilizes input from IDA ICE and tracks patterns with a system identification toolbox. The modeling utilizes the Matlab command $ssest$ for approximation. See Figure 5.8 for implemented method.

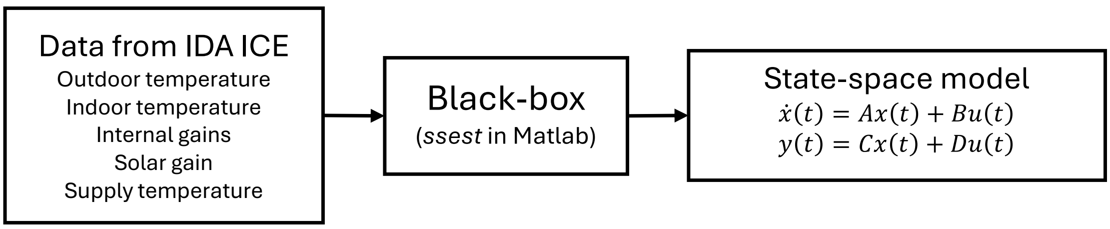

Figure 5.8: Workflow for creation of a black-box model.

The primary drawback of black-box models is the absence of physical parameters. Since the approach relies strictly on machine learning, the optimization process focuses solely on achieving the best possible mathematical fit. The resulting matrices lack a direct correlation to the building's physical properties and cannot be compared with hand calculations. This lack of physical parameters creates uncertainties regarding the model's reliability.

5.3.3 Grey-box model

A grey-box model is a mixture of white-box and black-box modeling. It combines the usage of physical parameters with assumed simplifications and an optimization algorithm. This method allows the model to utilize real building parameters while reducing manual labor for the designer. A grey-box model approach was suggested according to Figure 5.9 which is a lumped model with two volumetric heat capacities.

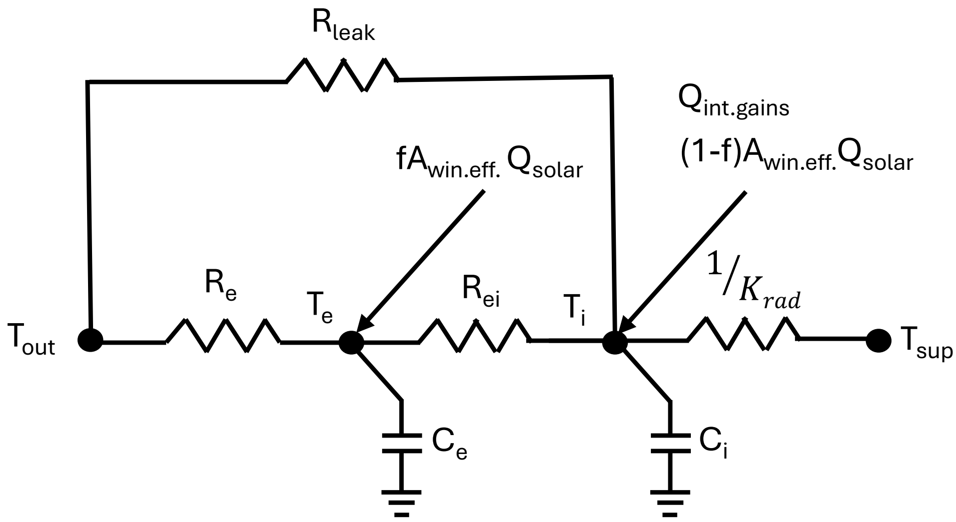

Figure 5.9: Grey-box circuit for one zone

Figure 5.9 utilizes the same notations as Figure 4.5. The model merges all elements that affect heat flow and capacity including walls, floor and roof in R_e and C_e. C_i denotes the volumetric heat capacity of the room including air, furniture and radiators. R_{ei} describes the convective resistance from the structure to the inside air. R_{leak} is the resistance for leakage in the building to the outside air. The constant f distributes the solar gains between the structure and indoor air and $A_{win.eff.}$ is a constant with the purpose to consider shading, area and direction of sun. Instead of calculating the constants resulting values, an optimization algorithm was created which utilized the measured indoor temperature from IDA ICE and minimized the offset by alternating C_e, C_i, R_e, R_{ie}, R_{leak}, f, $A_{win.eff.}$ and K_{rad} which is further explained in section 5.3.4. The differential equations describing the heat exchange are presented in Equations (5.1) and (5.2). Heat flows are presented in Equations (5.3) and (5.4)

$$T_{\text{in}}: \quad C_{\text{i}}\frac{dT_{\text{in}}}{dt} = \frac{T_{\text{e}} - T_{\text{i}}}{R_{ei}} + \frac{T_{\text{out}} - T_{\text{i}}}{R_{leak}} + K_{rad}(T_{\text{sup}} - T_{\text{i}}) + Q_i \tag{5.1}$$

$$T_{\text{e}}: \quad C_{\text{e}}\frac{dT_{\text{e}}}{dt} = \frac{T_{\text{i}} - T_{\text{e}}}{R_{\text{ei}}} + \frac{T_{\text{out}} - T_{\text{e}}}{R_{\text{e}}} + Q_e \tag{5.2}$$

$$Q_i = Q_{int.gains} + (1-f)A_{win.eff}Q_{solar} \tag{5.3}$$

$$Q_e = fA_{win.eff}Q_{solar} \tag{5.4}$$

Q_{solar} and T_{out} are retrieved from the climate file and $Q_{int.gains}$ is retrieved from IDA ICE heat balance. T_{sup} is the supply temperature of the water which was extracted from IDA ICE in a custom output file. K_{rad} is a constant for every radiator, optimized for every zone and considers the heat transfer to the room and the area of the radiators.

A radiator is described with two equations, the energy balance and the heat transfer to the room. The energy balance is proportional to the difference between the supply and return temperature as well as the mass flow of water described in Equation (5.5). The heat transfer to the room is dependent on the indoor temperature, which is proportional to the difference between the radiator's temperature and the indoor temperature, see Equation (5.6). Equations are derived from IDA ICE code.

$$Q_{rad} = \dot{m}c_p(T_{sup} - T_{ret}) \tag{5.5}$$

$$Q_{rad} = k_{rad}(T_{mean} - T_{in})^n \tag{5.6}$$

Where $\dot{m}$ is the massflow of water into the radiator [kg/s], c_p the specific heat capacity of water [J/kgK], T_{ret} the return temperature of the water [°C] and T_{mean} is the mean temperature of the radiator's surface calculated according to Equation (5.7). As seen in Equation (5.6), the temperature difference has a non-linear relationship towards the supplied heat with the exponent n [-]. This is caused by the radiator's efficiency increasing for higher temperatures and this relationship is what IDA ICE utilizes. Although, since a linear MPC is designed, the exponent cannot be used and was therefore neglected in the calculations.

$$T_{mean} = \frac{T_{sup} - T_{ret}}{2} \tag{5.7}$$

If T_{ret} is isolated from equation (5.5), it can be written according to equation (5.8)

$$T_{ret} = T_{sup} - \frac{Q_{rad}}{\dot{m}c_p} \tag{5.8}$$

By combining equations (5.7) and (5.8) a new expression for T_{mean} is achieved according to equation (5.9).

$$T_{mean} = T_{sup} - \frac{Q_{rad}}{2\dot{m}c_p} \tag{5.9}$$

By combining Equation (5.9) with Equation (5.6) an expression without dependence on the return temperature is achieved, see Equation (5.10).

$$Q_{rad} = k_{rad}(T_{sup} - \frac{Q_{rad}}{2\dot{m}c_p} - T_{in}) \tag{5.10}$$

By isolating Q_{rad} in Equation (5.10), it can be written according to Equation (5.11).

$$Q_{rad} = \frac{k_{rad}}{1 + \frac{k_{rad}}{2\dot{m}c_p}}(T_{sup} - T_{in}) \tag{5.11}$$

Since the control sequence utilized in the project is ideal when the valve is fully open, which is thoroughly explained in chapter 5.4, the massflow can be considered constant for the MPC. This assumption means that the fraction achieved in equation (5.11) is a constant and can therefore be expressed as K_{rad} in equation (5.1).

To create a state-space model, the stated differential equations were written on the correct form where Equation (5.12) represents the state vector x, Equation (5.13) represents the disturbance vector u, Equation (5.14) represents the system matrix A, Equation (5.15) represents the disturbance input matrix B, Equation (5.16) represents the output matrix C and Equation (5.17) represents the feedthrough matrix D.

$$x = \begin{bmatrix} T_i & T_e \end{bmatrix}^T \tag{5.12}$$

$$u = \begin{bmatrix} T_{out} & Q_i & Q_e & T_{sup} \end{bmatrix}^T \tag{5.13}$$

$$A = \begin{bmatrix} -\frac{(\frac{1}{R_{ei}}+\frac{1}{R_{leak}}+K_{rad})}{C_i} & \frac{1}{R_{ei}C_i} \\ \frac{1}{R_{ei}C_e} & -\frac{(\frac{1}{R_{ei}}+\frac{1}{R_e})}{C_e} \end{bmatrix} \tag{5.14}$$

$$B = \begin{bmatrix} \frac{1}{R_{leak}C_i} & \frac{1}{C_i} & 0 & \frac{K_{rad}}{C_i} \\ \frac{1}{R_eC_e} & 0 & \frac{1}{C_e} & 0 \end{bmatrix} \tag{5.15}$$

$$C = \begin{bmatrix} 1 & 0 \end{bmatrix} \tag{5.16}$$

$$D = \begin{bmatrix} 0 & 0 & 0 & 0 \end{bmatrix} \tag{5.17}$$

5.3.4 Optimization algorithm

For all zones, the parameters C_e, C_i, R_e, R_{ie}, R_{leak}, f, $A_{win,eff}$ and K_{rad} are not calculated with their respective properties. Instead, because of the amount of zones, the parameters went through an iterative optimization algorithm. The thesis utilized the built-in function $minimize$ from the SciPy library, which iteratively minimizes J in equation (5.18) by alternating values in θ from (5.19). The script utilized for optimization is attached in Appendix B.

$$J(\theta) = \frac{1}{N}\sum(T_{sim}(\theta,t) - T_{measured}(t))^2 \tag{5.18}$$

Where

$$\theta = \begin{bmatrix} C_e & C_i & R_e & R_{ie} & R_{leak} & f & A_{win.eff.} & K_{rad} \end{bmatrix} \tag{5.19}$$

Where N denotes the amount of time steps in the data, T_{sim} is the resulting indoor temperature when simulating the state-space model and $T_{measured}$ is the real indoor temperature.

To avoid optimizing into local minima and to achieve parameters connected to the physics of the zones, constraints evaluated from hand-calculations were applied according to Table 5.1.

Table 5.1: Constraints for the physical parameters for the grey-box model, including hand-calculated estimates for an arbitrary zone.

Parameter	Lower boundary	Upper boundary	Hand-calculations
C_e	$3 \cdot 10^7$	$7 \cdot 10^8$	$4.4 \cdot 10^7$
C_i	$8 \cdot 10^5$	$2 \cdot 10^7$	$4.8 \cdot 10^5$
R_e	10^{-3}	10^{-1}	$5.0 \cdot 10^{-2}$
R_{ei}	10^{-3}	10^{-2}	$4.2 \cdot 10^{-2}$
R_{leak}	10^{-3}	10^{-2}	–
f	0.1	0.9	–
$A_{win.eff}$	0.5	35	–
K_{rad}	90	170	–

Table 5.1 displays the upper and lower boundaries accompanied with the estimated hand-calculations for an arbitrary zone in the building. The hand-calculations marked with a hyphen are values which are not connected to equations, but rather parameters to aid the optimization algorithm in understanding the solar gains, radiators' and ventilation's effect on the indoor temperature. When calculating C_e, all exterior elements were considered, including walls, roof and floor. C_i considers the indoor air and furniture inside. R_e includes the surface resistance between the outdoor air and facade as well as all building materials in the exterior elements. R_{ei} is the surface resistance between the interior surfaces and the indoor air. R_{leak} is a parameter which aids the optimization algorithm to understand how the air to air heat transfer occurs, mainly regarding leakage and ventilation.

The lower and upper boundaries in Table 5.1 were iteratively evaluated. Note that the volumetric heat capacity for the indoor temperature node has boundaries beyond the hand-calculations. This is a consequence of the leakages added in the model which caused the optimization algorithm to compensate into a larger capacity than anticipated.

5.3.5 Model evaluation

The implementation of white-box model in each zone is time consuming and since the evaluated building consists of more than 100 zones the method was deemed insufficient. The following study will therefore compare grey-box and black-box models.

An arbitrary zone was used for the comparison which yielded the result presented in Figure 5.10. The simulation was carried out with a fluctuating supply temperature to the radiators along with fully opened valves, hence the large fluctuations and high temperatures.

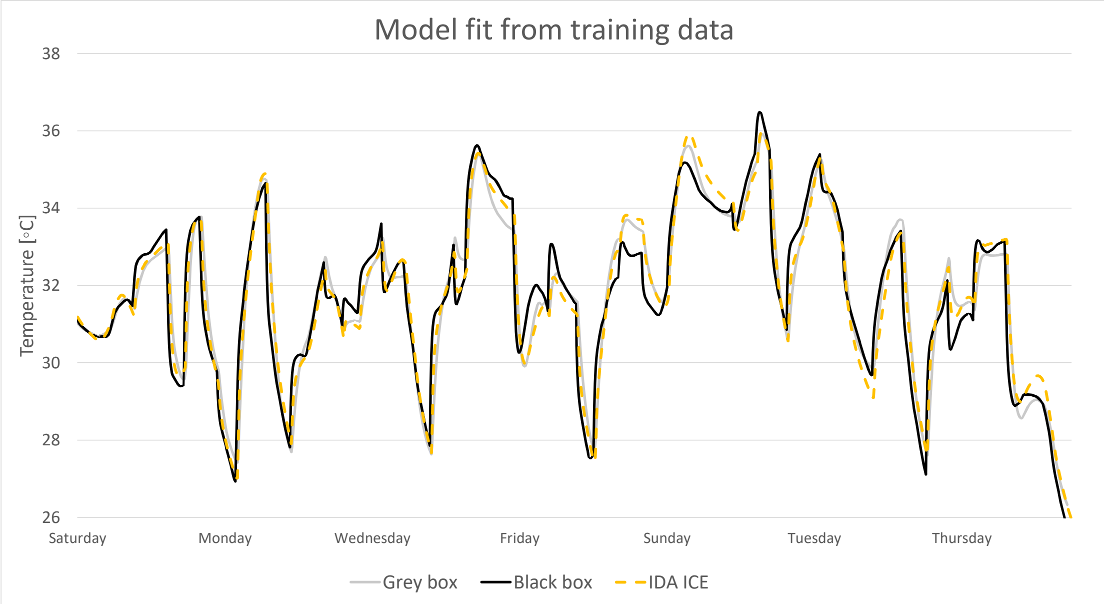

Figure 5.10: Comparison between measured, grey-box and black-box modeling during two weeks in march after optimization in one arbitrary zone in the building.

As viewable in Figure 5.10 both models follow the corresponding temperature trend of the zone and has comprehended the dynamics of the zone. However, to scientifically distinguish the models in detail, the root mean square error ($RMSE$) and normalized root mean square error ($NRMSE$) have been used. The $RMSE$ calculates the average error for the model in degree celcius according to Equation (5.20) and $NRMSE$ normalizations makes it possible to compare zones whom differentiate in temperature span and is calculated according to Equation (5.21).

$$RMSE = \sqrt{\frac{1}{n}\sum_{i=1}^{n}(\hat{y}_i - y_i)^2} \tag{5.20}$$

$$NRMSE = \frac{RMSE}{y_{max} - y_{min}} \tag{5.21}$$

The resulting $RMSE$ and $NRMSE$ are presented in Table 5.2.

Table 5.2: Comparison of model fit to measured temperature for Grey-box and Black-box approaches for one arbitrary zone in the building.

Method	RMSE [°C]	NRMSE [%]
Grey-box	0.34	83.68
Black-box	0.31	85.19

In Table 5.2, the RMSE of the grey-box model ends up at an average of 0.34 °C difference for the simulation period and the black-box model at 0.31 °C difference. The grey-box presents a 83.68 % match whilst the black-box fulfills a 85.19 % match. The conclusion is that the black-box model performs slightly better than the grey-box model.

Although, since the black-box model depends on machine learning and no physical parameters it is not certain it has understood how each disturbance affect the zone. To verify this, the training signal was substituted to a different control signal. The results can be observed in Figure 5.11

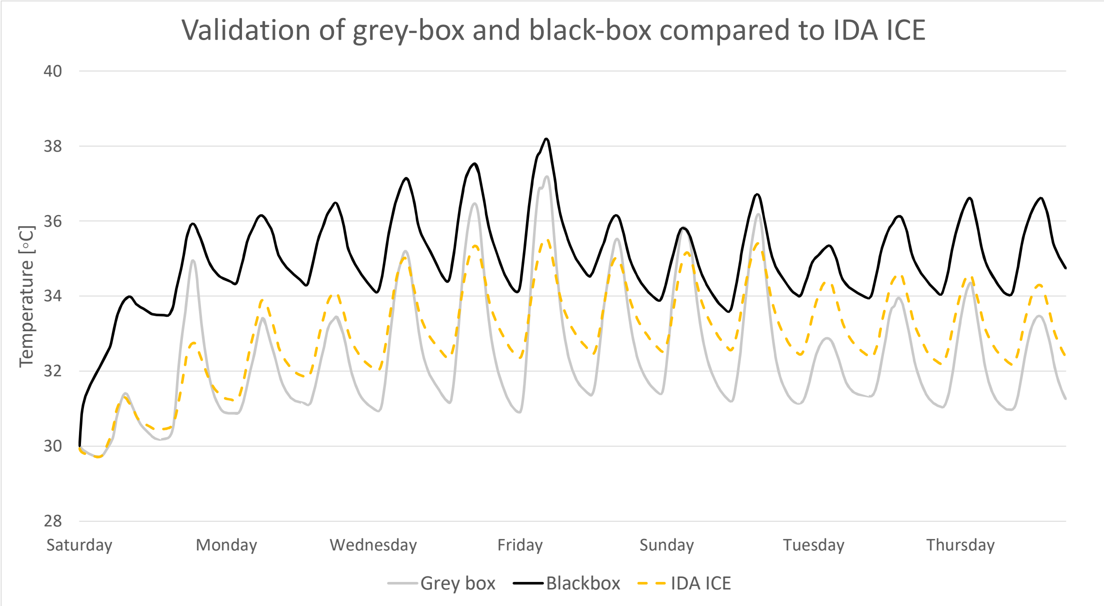

Figure 5.11: Comparison between measured, grey-box and black-box modeling during two weeks in March with a constant control supply temperature of $40°C$ and fully opened valves.

As illustrated in Figure 5.11, neither model achieves a particularly close fit to the reference data from IDA ICE. However, the grey-box model demonstrates a higher degree of alignment with the measured temperatures, despite its tendency to occasionally overshoot peaks and undershoot valleys. The black-box model tracks the general temperature trends but it maintains a constant error, suggesting that certain physical behaviors are not captured by the model. Based on these observations, the grey-box model was selected for the remainder of this project for prediction of temperatures for the MPC.

5.4 Control scheme

Due to the complexity of the reference model, a subset of zones was selected for the control scheme. Certain zones exhibited dynamics that were too complex for the simplified model structure, resulting in model fits that were deemed insufficient for reliable control. The highlighted zones in Figure 5.12 were chosen based on an indoor temperature analysis of the entire building which revealed them to be the most critical and therefore representing the worst-case scenario zones for the control system.

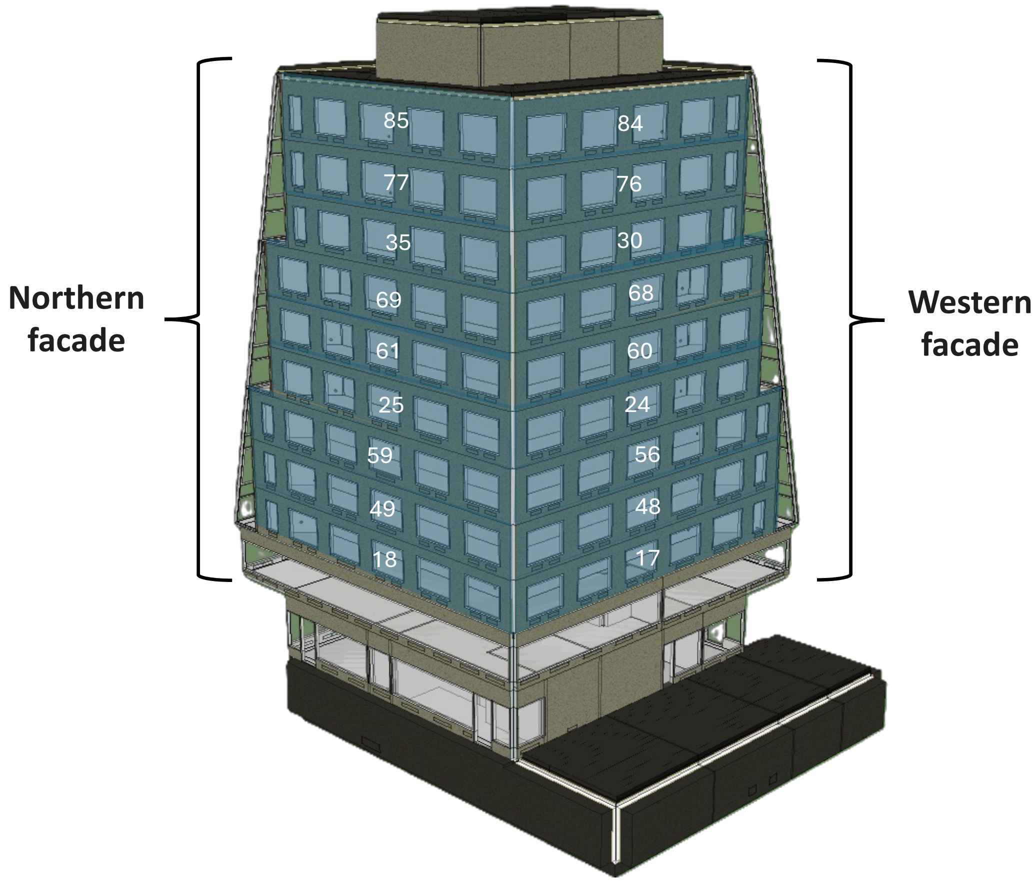

Figure 5.12: Reference model in IDA ICE where the controlled zones are highlighted.

The control scheme of the heating system is divided into two main parts, the MPC and the IDA ICE simulation environment. Figure 5.13 displays the optimization taking place for every time step of 15 minutes.

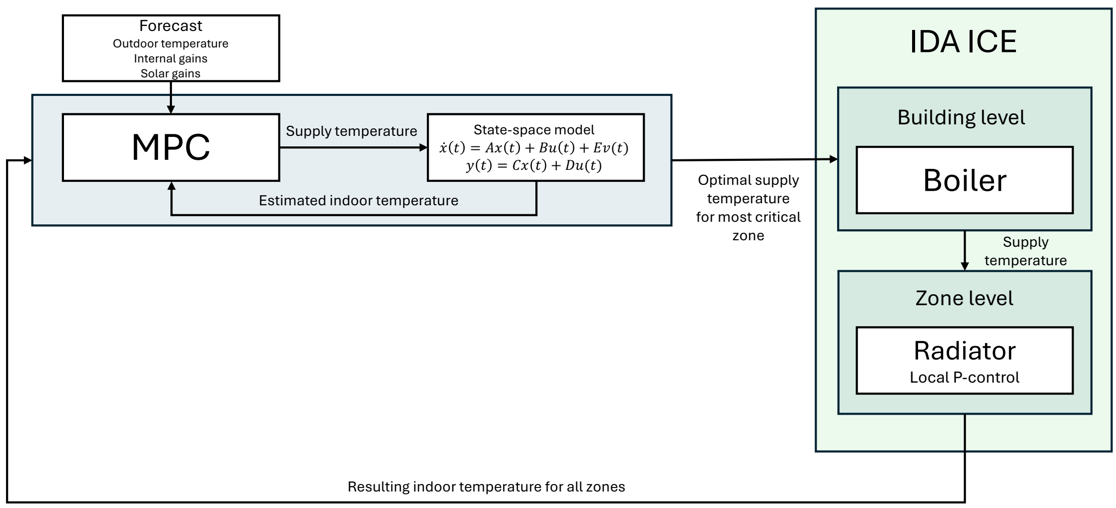

Figure 5.13: Control scheme of the heating system.

As seen in Figure 5.13, the control sequence is initiated by importing the indoor temperature for all the controlled zones and the MPC selects the most critical zone, meaning the lowest temperature zone, to base the supply temperature on. Secondly, the forecast is fed into the MPC containing outdoor temperature, internal gains and solar gains. Different supply temperatures are suggested to the state-space model which calculates the estimated indoor temperature and sends it back to the MPC. After enough iterations the MPC finds the most optimal supply temperature to export to the boiler in IDA ICE. The boiler distributes the supply temperature to all radiators with thermostats and P-controllers with a P-band of 1.5°C. The previous indoor temperature's offset from the reference temperature is evaluated and an individual valve opening is calculated for every radiator. IDA ICE then simulates the resulting indoor temperature for all zones which is exported to the MPC and the loop restarts with the new state for the most critical zone. See Appendix B for detailed code of the co-simulation.

The state-space models, whose purpose is to predict the indoor temperature, were trained with a fully opened valve which means a constant maximum mass flow of water. The MPC's optimal supply temperature will therefore be based on a fully opened valve in the most critical zone.

The co-simulation with IDA ICE was executed by creating a schematic of the building in the software. A schematic is a model which describes how all components are connected with their respective equations, variables and parameters. An example of a schematic with co-simulation for two zones is presented in Figure 5.14.

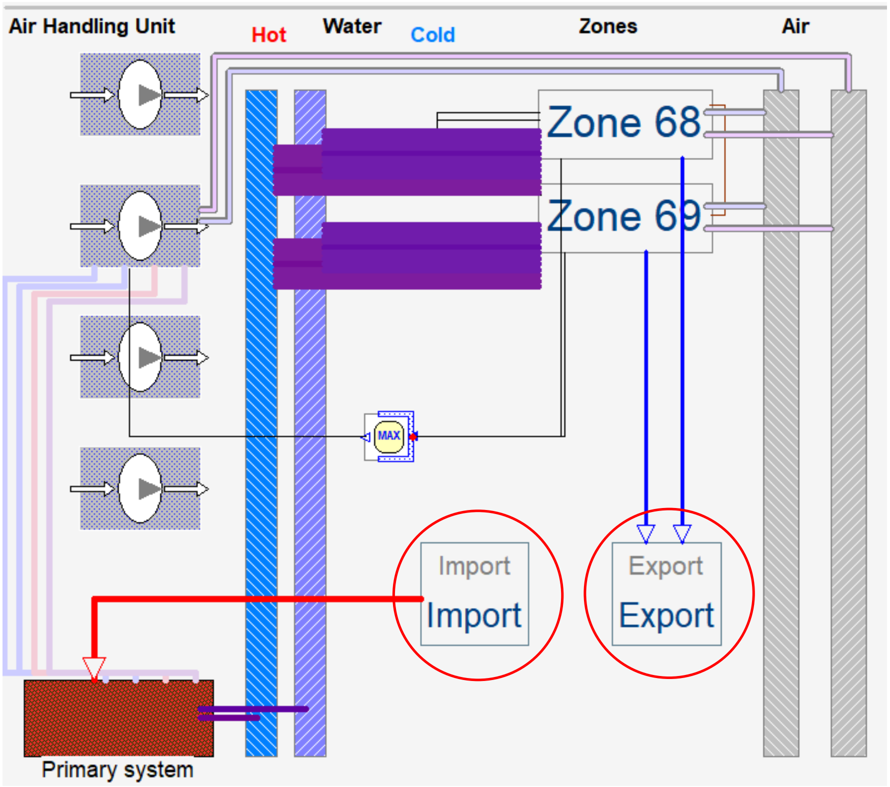

Figure 5.14: Setup of the co-simulation control scheme for two arbitrary zones in IDA ICE in the main schematic.

The schematic for the co-simulation framework with IDA ICE is illustrated in Figure 5.14. The blue signal lines originating from the zones transmit the indoor temperature data to the export block, which sends the temperature measurements to the MPC algorithm running within the Python environment. The optimized supply temperature calculated by Python is fed back via the import block, where the red signal line supplies the primary system with the optimized supply temperature. The detailed schematic of this primary system is further presented in Figure 5.15.

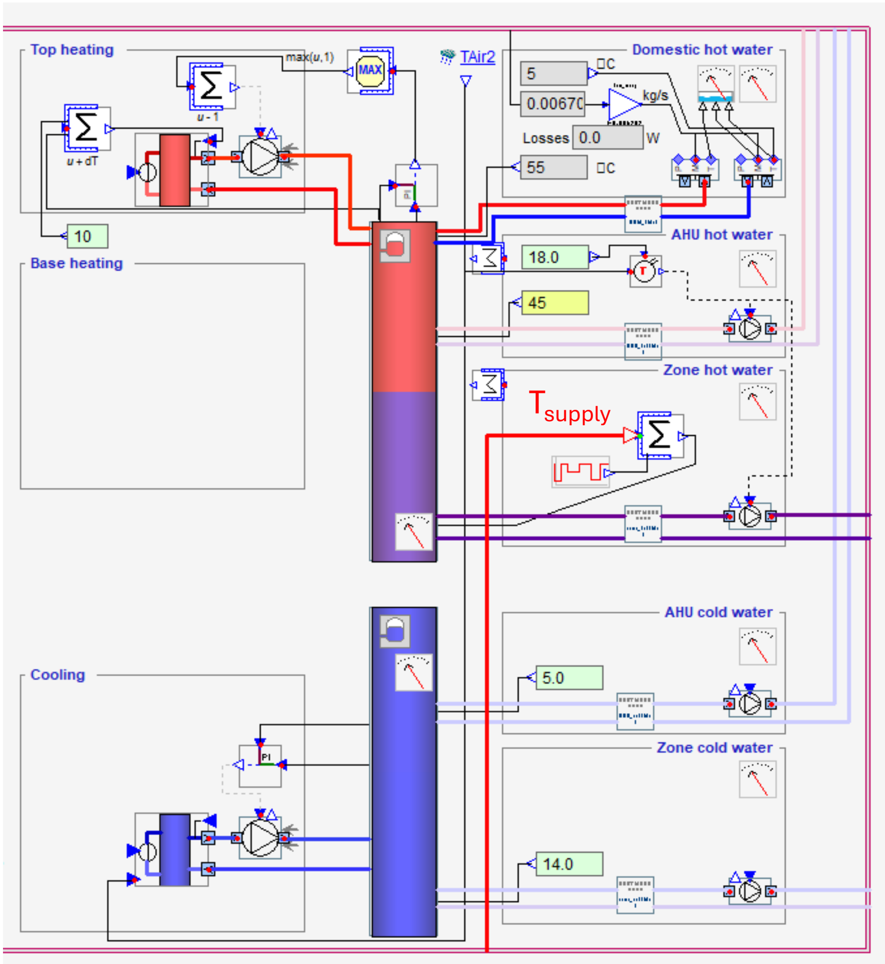

Figure 5.15: Setup of the co-simulation control scheme in IDA ICE in the primary system.

The primary system in Figure 5.15 contains schematics for top heating, domestic hot water, air handling unit hot water, zone hot water, air handling unit cold water and zone cold water. The boiler and cooler for the building are displayed in the center. For the co-simulation, the red line named T_{supply} is connected to the zone hot water segment which along with the operation schedule sends a supply temperature to the boiler.

5.5 Forecast uncertainty

The considered MPC in the thesis relies on forecasts for weather and occupancy. Forecasts are based on probability, meaning the possibility for errors are apparent. Regarding weather forecasts, the uncertainties mainly emerge from simplifying areas into grids, the amount of data points, deciding initial states and non-linearity in the atmosphere (SMHI, n.d.-a). The non-linearity in the atmosphere creates a chaotic system which is a system who's initial conditions has remarkable effect in the forecast. When forecasting weather, the chaotic characteristics causes the error to increase over simulation time, meaning a forecast which is further away in time is less trustworthy. According to SMHI (n.d.-b), the accuracy of a 24-hour forecast is 84% for temperature which is defined as less than 2°C difference between forecast and measured value (SMHI, 2025). To account for the forecast error a custom climate file was created which considers the standard deviation in temperature. If it is assumed that the temperature deviates equally, meaning as often as the temperature is overrated it is underrated, the distribution ends up at 84% in the 2°C span, 8% below and 8% above. The assumed normal curve is plotted in figure 5.16.

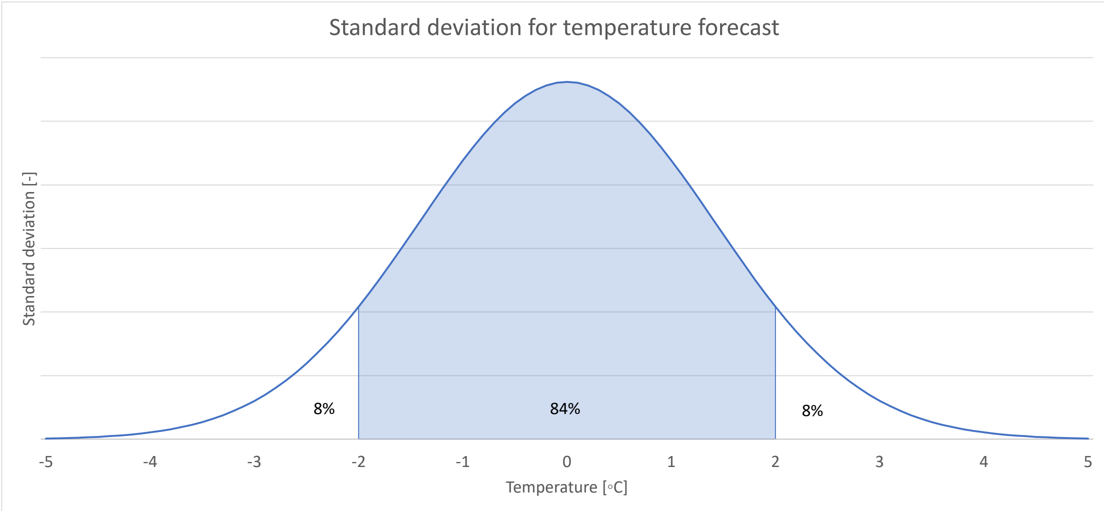

Figure 5.16: Assumed normal curve according to data from SMHI (2025).

By combining the standard deviation with a function which randomly assigns a probability between 0 and 1 the forecast error is simulated. The resulting manipulated forecast is presented in figure 5.17.

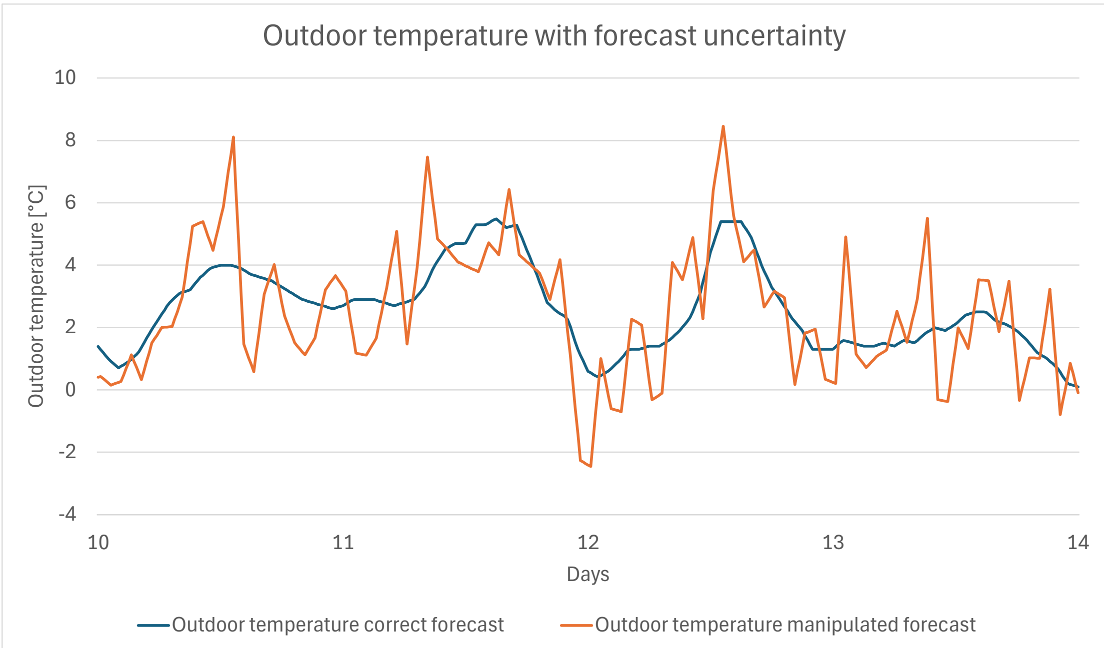

Figure 5.17: Deviating outdoor temperature from actual outdoor temperature.

Regarding occupancy behavior, difficulties emerge when simulating since the patterns of behavior are irregular. To account for irregular occupant behavior, all office zones will be assigned schedules which reduces the occupancy by 50 % compared to what the MPC has forecasted. Schedules which account for uncertainty are displayed in Figures 5.18a and 5.18b.

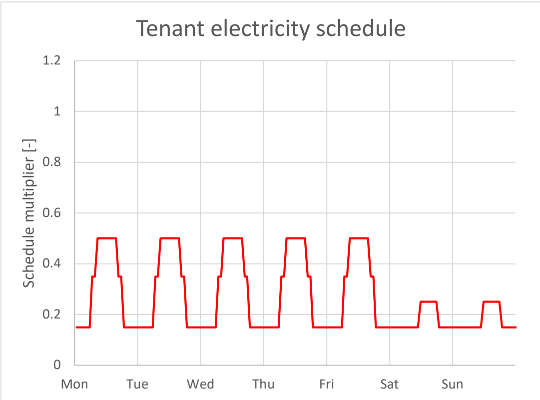

(a) Reduced schedule for tenant electricity applied in IDA ICE.

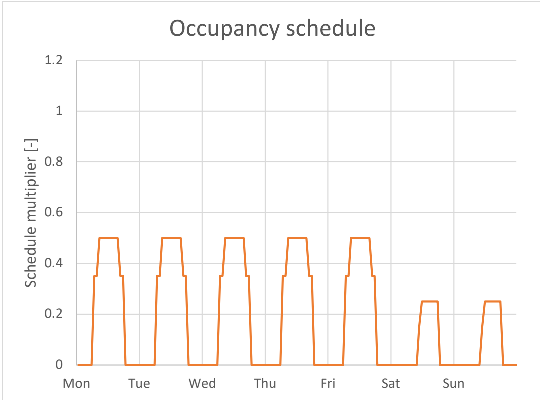

(b) Reduced schedule for occupancy applied in IDA ICE.

Figure 5.18: Schedules used in IDA ICE applied on the office areas, reduced with 50% from schedules presented in Figures 5.6a and 5.6b.

6 Results

The results for the thesis are presented in this chapter. The model fit between IDA ICE, on-site measurements and state-space models are evaluated along with the resulting analysis from the MPC simulations.

6.1 Model fit to reality

To evaluate if the building performs according to reality, the on-site measurements for heating, cooling and ventilation electricity regarding power and energy have been compared to the simulated values from IDA ICE. Figure 6.1 displays the total heating power over one year. The IDA ICE model underestimates the actual energy usage, mainly during January, February and March. However, the behavior of the heating in the building is well replicated with peak demands aligning. Although, the model does not consider the power from curtain heaters, losses from control systems or loss of heat because of airing towards the terrace, which is considered for the total energy usage.

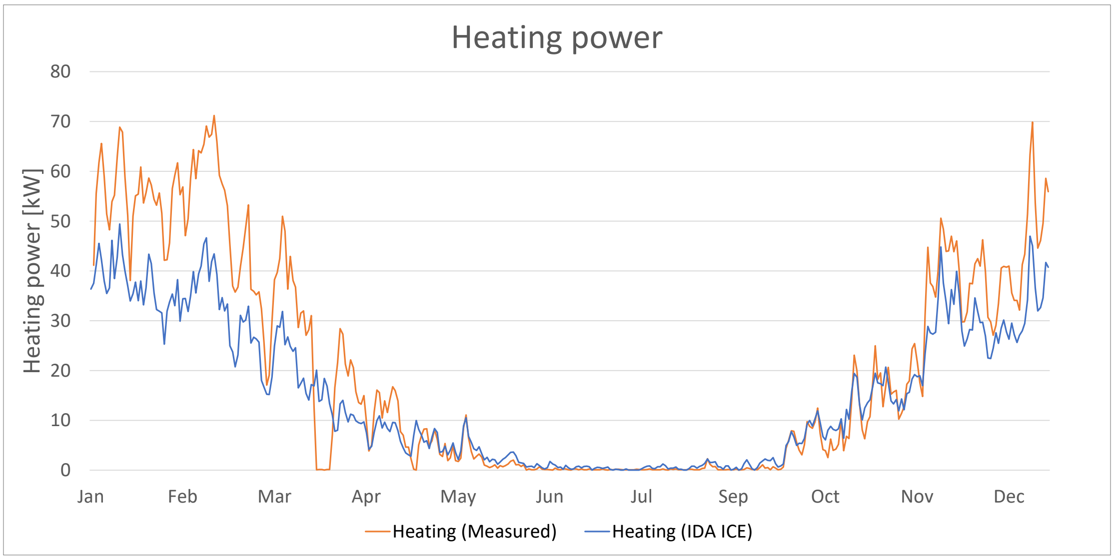

Figure 6.1: Heating power in the building during 2025. The orange line displays the on-site measurements and the blue line shows the results from simulation

The cooling power throughout the year was also evaluated and presented in Figure 6.2. The cooling power is not well adapted to the on-site measurements regarding amplitude but appears to follow the correct behavior. When power peaks emerge, both the measurements and simulations align but the simulated cooling has on average a greater magnitude. The difference between simulation and on-site measurements could be a consequence of the behavior of the tenants such as airing, vacation during summer months, vacant floors or air handling units operating differently in reality.

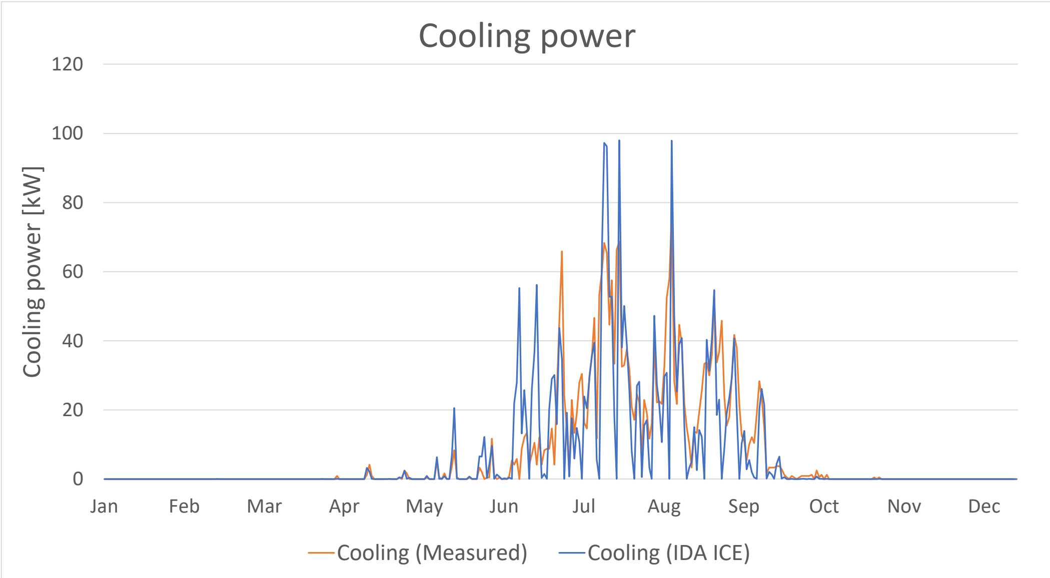

Figure 6.2: Cooling power in the building during 2025. The orange line displays the on-site measurements and the blue line shows the results from simulation.

The final evaluation consisted of comparing the total energy usage during 2025 for heating, cooling and ventilation electricity. The results are presented in Figure 6.3.

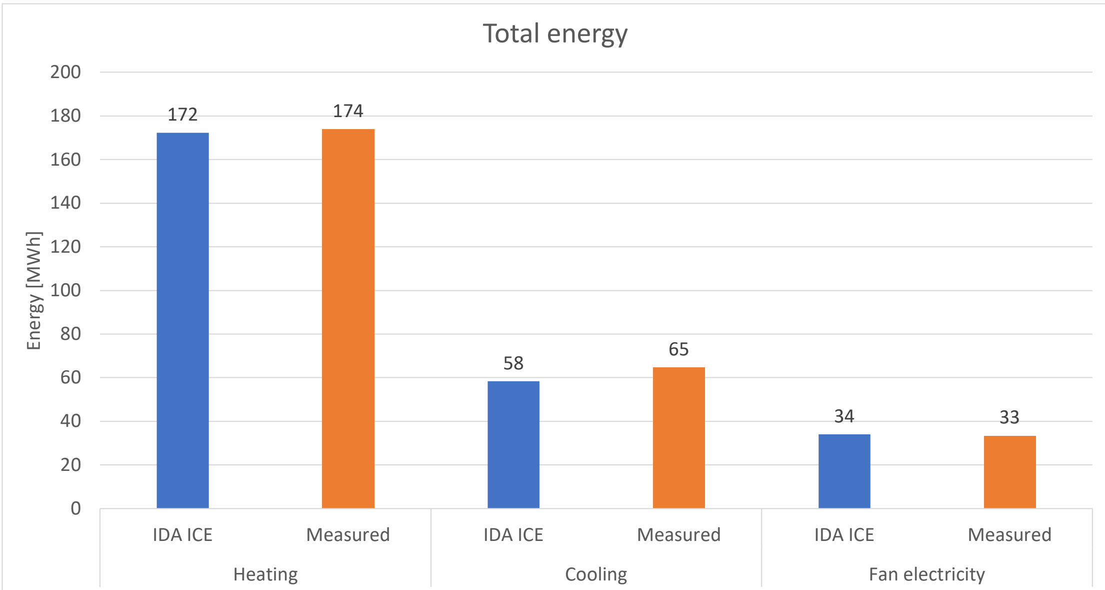

Figure 6.3: Total energy during 2025, expressed in MWh for heating, cooling and ventilation electricity. The orange bars displays the on-site measurements and the blue bars shows the results from simulation.

The heating displays a good fit between the simulation and measured values in figure 6.3. The simulated heat was increased with 1 kWh/m^2A_{Temp} to account for window-opening in the building. The value was evaluated from the standard value from Boverket (2017) of 4 kWh/m^2A_{Temp} but was lowered since windows cannot be opened in the building except for the terrace doors. Additionally the total simulated heating was increased 10% to account for losses in the control and distribution system (Personal communication, Gustav Thuresson). Finally a standard value for the five curtain heaters above the entrances was added according to the guidelines from Sveby (2010), 4 MWh per curtain heater. The resulting difference between the total heating energy was approximately 2 MWh/year, which is a 1.2% difference.

The total cooling is greater for the on-site measurements with a difference of 10.8%. The ventilation electricity has a difference of 9.7% with the simulated electricity surpassing the measured. However, since the restaurant which opened after half of the simulation period increased the air flows, the behavior during the first six months was repeated throughout the entire year. Additionally, the energy meter was connected to three electric radiators, the main elevator and an elevator from the basement to the entrance floor. This was handled by subtracting the simulated heating energy of 1.5 MWh/year from the measured value along with subtracting the assumed elevator electricity of 5.5 MWh/year according to Sveby (2010). The difference when evaluating the ventilation electricity could be the consequence of different settings in the air handling unit in reality.

6.2 Model fit to state-space models

The resulting model fit has been evaluated by calculating the resulting RMSE and NRMSE from simulated temperatures against measured temperatures from IDA ICE. The models are validated by also comparing the resulting volumetric heat capacity and thermal resistance after optimization. The evaluated zones in the building are presented in Figure 6.4.

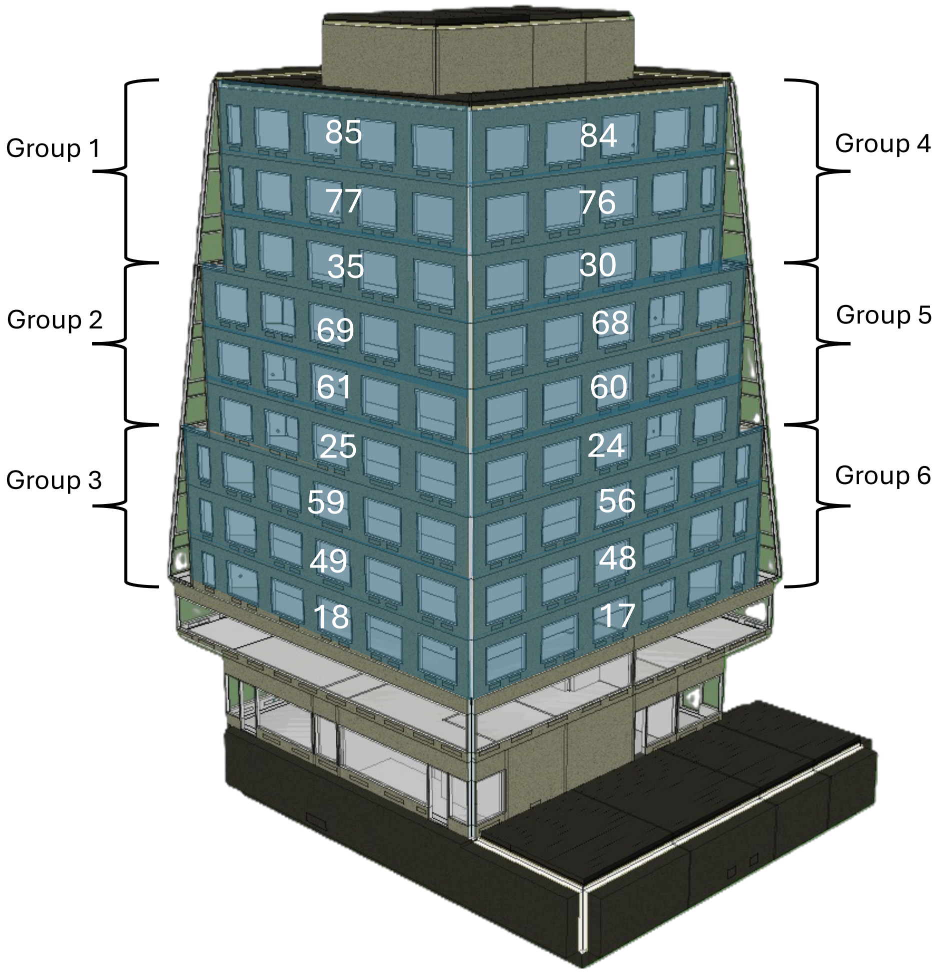

Figure 6.4: Zone numbers for the northern and western facade.

As seen in Figure 6.4, the zones are of three different sizes on the northern and western facade. This resulted in 6 different groups of zones with equivalent properties because of equal volumes and areas. However, different conditions for all individual zones are apparent due to variations in area which transmits heat from above and below. Additionally, the increased solar gain for higher elevated zones creates differences because of surrounding shading objects. The conclusion is that all zones are unique and needed to be evaluated individually. The resulting RMSE and NRMSE from simulations for all zones numbered in Figure 6.4 with group numbers are displayed in Table 6.1.

Table 6.1: Model fit performance expressed as RMSE and NRMSE for each zone on the northern and western facade, updated with the latest optimization results.

Group	Zone	RMSE [°C]	NRMSE (%)
Northern facade			
	Zone 18	0.39	75.90
Group 1	Zone 49	0.41	75.11
	Zone 59	0.43	74.92
	Zone 25	0.42	74.63
Group 2	Zone 61	0.43	74.56
	Zone 69	0.43	75.00
	Zone 35	0.43	75.05
Group 3	Zone 77	0.43	75.07
	Zone 85	0.39	78.26
Western facade			
	Zone 17	0.48	73.79
Group 4	Zone 48	0.52	71.34
	Zone 56	0.56	70.19
	Zone 24	0.56	69.50
Group 5	Zone 60	0.56	69.59
	Zone 68	0.57	69.81
	Zone 30	0.57	69.52
Group 6	Zone 76	0.57	69.98
	Zone 84	0.52	74.44

The second column in Table 6.1 displays an average error between 0.39 to 0.57°C. The total average error for all zones regarding RMSE was calculated to 0.48°C. It is evident that the zones on the western facade exhibit a lower fit which is likely a consequence of the higher exposure to solar radiation. The solar load introduces complex thermal dynamics that are more challenging for the model to accurately capture. As for the NMRSE, which can be expressed as the model fit compared to IDA ICE, the values ranges from 69 to 78%. In terms of model fit of building zones, these values can be considered acceptable.

To evaluate the credibility of the state-space models, the resulting parameters after optimization are displayed in Appendix C along with the parameters calculated by hand as a comparison.

6.3 Model predictive control

The developed model predictive controller was tested for three scenarios, each prioritizing a different control objective. However, in all three scenarios, it was important that the indoor comfort was maintained. In the first scenario, the primary goal was to minimize overall energy usage, which was achieved by heavily penalizing high supply temperatures in the cost function. The second scenario focused on peak shaving by assigning a dominant weight to the rate of change of the supply temperature. Finally, the objective of the third scenario was to maintain thermal comfort, meaning the penalty for deviating from the temperature setpoint was the dominant factor.

The simulation period was limited to two weeks to increase computational speed. March was selected as the timeframe, as it represents a transitional period with significant heating demand combined with substantial solar gains. To better showcase the results and to ensure that the model has converged only the second week is plotted in the coming figures.

6.3.1 Setup and constraints

To find the optimal weights and constraints the MPC were simulated multiple times as an iterative process. The final weights of the cost function can be found in Table 6.2.

Table 6.2: Cost function weights and penalties for the three simulation scenarios where w_y penalizes temperature deviations, w_v is pressuring the boiler to a lower supply temperature, $w_{\Delta v}$ penalizes rapid change of supply temperature and w_s ensures that the MPC stays within the temperature boundaries.

Simulation	w_y	w_v	$w_{\Delta v}$	w_s
Energy saving	20	800	600	10 000
Peak shaving	400	100	40 000	10 000
Thermal comfort	9500	0.1	1000	10 000

As presented in Table 6.2, the weights were adjusted to reflect the specific objectives of each simulation scenario. However, the penalty for constraint violations, w_s, remained constant across all simulations to ensure thermal stability. Furthermore, the operational constraints of the MPC are detailed in Table 6.3.

Table 6.3: Operational boundaries and constraints. The supply temperature, v, is a hard constraint, while the indoor temperature, y, is a soft constraint regulated by w_s.

Constraint Category	**Symbol**	**Value/Range**
Supply temperature (Hard)	v	$[23.0, 45.0]$ °C
Indoor temperature (Soft)	y	$[21.0, 25.0]$ °C
Target deadband (y_{ref})	$[y_{min}, y_{max}]$	$[21.9, 22.3]$ °C

The supply temperature constraints were given based on the technical specification provided by the property owner. Since the cooling setpoint for most zones in the building is set to 23 °C, the lowest supply temperature was set to the same value to prevent unintentional cooling from the radiators when indoor temperature exceeds supply temperature. The indoor temperature constraints were set based on the setpoints from the original IDA ICE model. The constraints are modeled as soft but with a high weight meaning the MPC should rarely break the boundaries. Instead of using a distinct setpoint, a target deadband was introduced to enhance controller stability while still maintaining adequate indoor climate. For example, during the thermal comfort simulation w_y was set high meaning that the MPC should prioritize to maintain the indoor temperature within the deadband.

6.3.2 Supply temperature analysis

The resulting weights and constraints were utilized to conduct a comprehensive analysis of the MPC. To evaluate its impact on the supply temperature, all three scenarios were plotted in Figure 6.5 alongside the traditional supply temperature curve. To better understand the impact from outdoor conditions, solar radiation and outdoor temperature is also displayed.

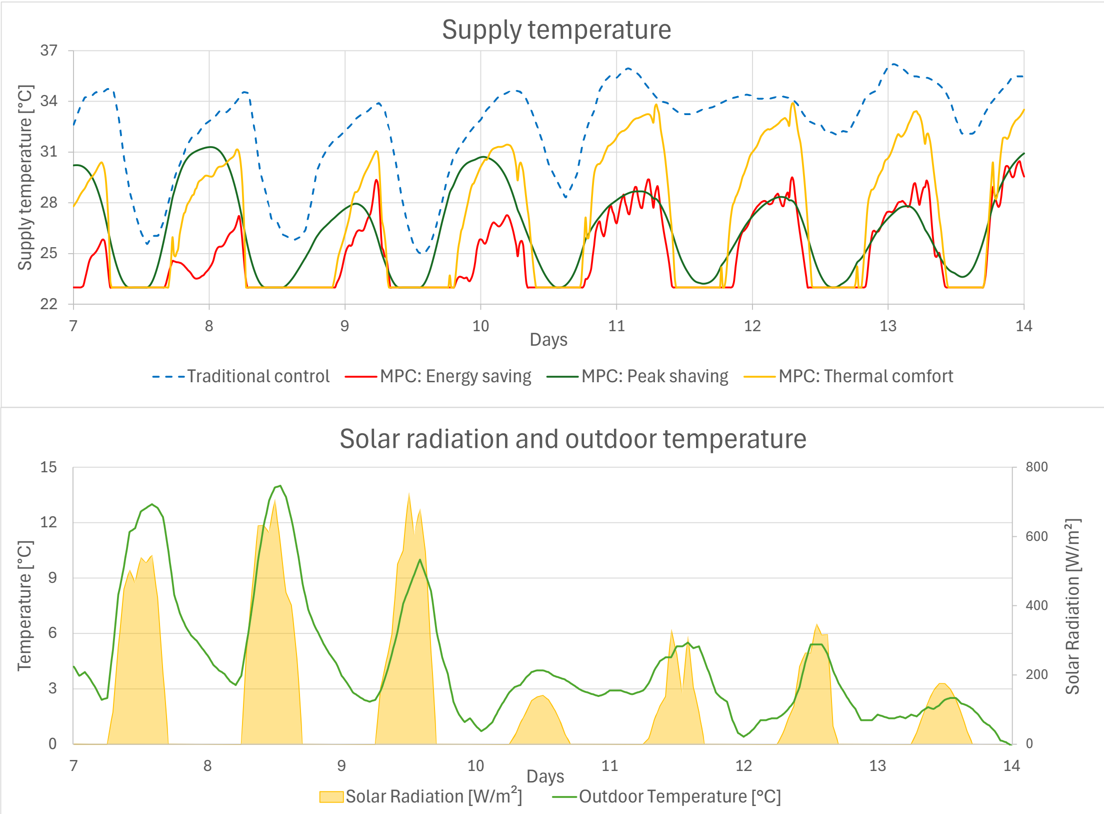

Figure 6.5: Top figure displaying resulting supply temperatures during one week for a traditional supply temperature curve, MPC with peak shaving, MPC with energy saving and MPC to maintain thermal comfort. Bottom figure displaying outdoor conditions for solar radiation and outdoor temperature during the same week.

As illustrated in the top graph of Figure 6.5, all three MPC scenarios generally maintain a lower supply temperature compared to the traditional control. While the traditional curve strictly follows the outdoor temperature as defined in Figure 5.3, the MPC continuously tries to optimize the supply temperature in different ways depending on what objective is set. Consequently, the results indicate that the radiators operate with a higher valve opening when operating under MPC control compared to the predetermined supply temperature curve.

The predictive performance of the MPC is validated by its proactive adjustment of supply temperatures. By accounting for upcoming solar radiation and rising outside temperature, it lowers the supply temperature hours before the predetermined supply temperature curve would otherwise dictate.

Moreover, the thermal comfort simulation maintains the highest supply temperature among the MPC scenarios, which agrees with its objective function. Although the energy-saving scenario may initially appear to outperform the peak-shaving scenario, this is due to the higher penalty weights assigned to temperature deviations in the peak-shaving configuration. The energy-saving simulation utilizes the full range of the comfort zone (21–25°C) to minimize energy use, resulting in a lower supply temperature. However, the trade-off is a lower average indoor temperature compared to the peak-shaving simulation. More about this in the following section.

6.3.3 Indoor temperature analysis

Following the analysis of the supply temperature, the indoor climate must be verified to ensure compliance with the established comfort limits. Figure 6.6 illustrates the average indoor temperature for the entire building across all three scenarios, compared against traditional control in IDA ICE.

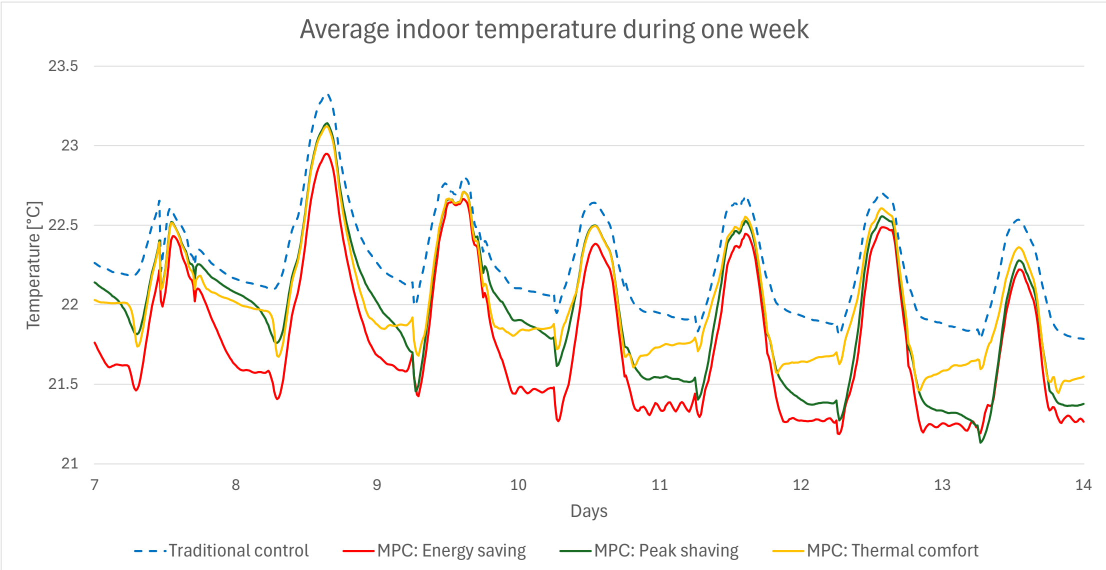

Figure 6.6: Average indoor temperature during one week for traditional control, MPC with peak shaving, thermal comfort and energy saving weights.

As illustrated in Figure 6.6, the traditional control maintains the highest average indoor temperature throughout the week. The thermal comfort simulation proves most effective at stabilizing the temperature around the setpoint (22°C). In contrast, the energy-saving simulation recorded the lowest average temperature, which aligns with the lower supply temperature observed in Figure 6.5.

While the temperature setpoints remained identical across all four simulations, the MPC allows for a lower average temperature within the comfort zone, whereas the traditional control rarely deviates below 22°C. To ensure a fair comparison, a separate traditional control baseline was simulated with an average temperature equivalent to that of the MPC simulations. This approach isolates the impact of the smart control from the savings simply gained by a reduction in indoor temperature. This will be evaluated in the following section.

6.3.4 Energy performance

To evaluate the energy performance of the various MPC strategies, zone heating demand was extracted from IDA ICE for the two-week simulation period. Initially, the standard traditional control was compared against the three MPC scenarios, as summarized in Table 6.4.

Table 6.4: Summary of heating energy, average indoor temperature, and energy savings for the different simulation scenarios.

Simulation	Heating energy [kWh]	Average indoor temp. [°C]	Savings [%]
Traditional control	5177	22.47	-
MPC: Energy saving	3475	22.13	32.88%
MPC: Peak shaving	3838	22.23	25.86%
MPC: Thermal comfort	4169	22.28	19.47%

As indicated in Table 6.4, the energy savings are substantial. However, the traditional control maintains a higher average indoor temperature compared to the MPC simulations. Normally, such marginal differences in average temperature would not yield savings of this magnitude. An analysis of the sensible energy balance in IDA ICE provides the explanation, see Appendix D. The lower average indoor temperature leads to a reduction in transmission losses through the building envelope and thermal bridges while simultaneously increasing the heat release from internal masses as a consequence of larger fluctuations in the indoor temperature. Furthermore, the traditional control simulation exhibits a slightly higher airflow and lower supply air temperature on average compared to the MPC simulations, further contributing to the increased heating demand. It is also of importance to consider the conditions for the simulations where two weeks in march, with temperature variations between 0 and 14°C and relatively high solar gains, contributes to increased percentage savings. These conditions result in a low heating demand where the control logic from the MPC becomes increasingly significant. The substantial savings are further discussed in section 7.1.

To ensure an equal evaluation and isolate the impact of the control logic from the effects of temperature reduction, the setpoint of the traditional control was adjusted to match the average indoor temperature of the different MPC scenarios. The results of this comparison is presented in Table 6.5.

Table 6.5: Comparison between traditional control with lower setpoints and MPC scenarios to isolate the impact of the control logic.

Simulation	Heating energy [kWh]	Average indoor temp. [°C]	Savings [%]
Traditional control (lower setpoint)	4301	22.28	-
MPC: Thermal comfort	4169	22.28	3.07%
Traditional control (lower setpoint)	4073	22.23	-
MPC: Peak shaving	3838	22.23	5.77%
Traditional control (lower setpoint)	3621	22.13	-
MPC: Energy saving	3475	22.13	4.03%

With the temperature discrepancy eliminated, the actual savings that the MPC provides becomes evident (3 - 5%). Interestingly, the peak shaving scenario emerges as the top performer. This is likely due to the fact that the energy saving scenario operates at a lower average temperature, resulting in fewer heating periods. When heating demand is already minimized, the relative margin for further optimization compared to the traditional control naturally diminishes.

The savings from the MPC are founded in the controller's anticipatory capabilities, such as adjusting the supply temperature in advance before solar radiation peaks or accounting for scheduled changes in occupancy. By proactively managing the building's thermal inertia, the MPC optimizes energy use in a way that reactive systems, such as the traditional control, cannot replicate.

6.3.5 Peak shaving

To analyze the potential for peak power shaving, the heating power demand was plotted over a one-week period, as illustrated in Figure 6.7.

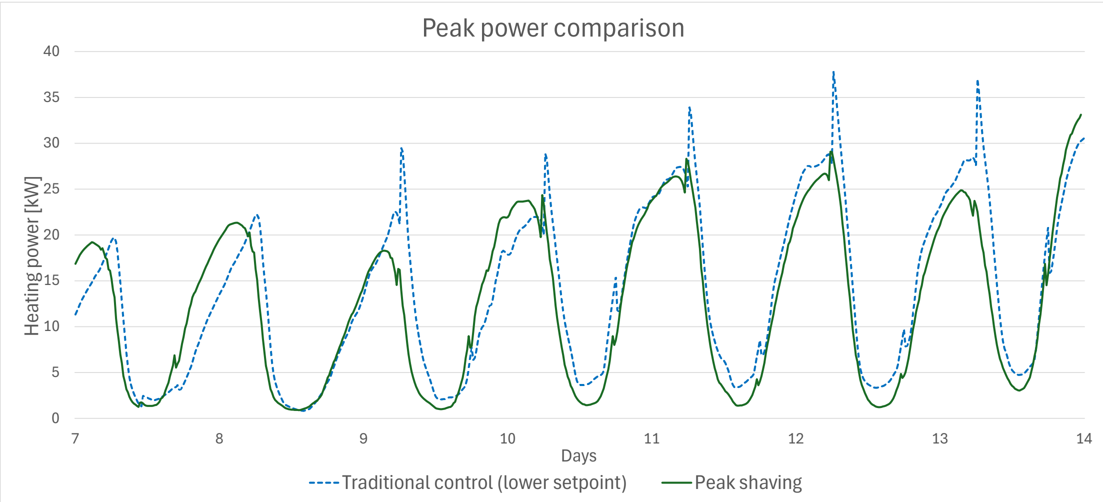

Figure 6.7: Heating power during one week for MPC with peak shaving settings and traditional control with equal average temperature.

A comparison between the MPC with peak shaving settings and the traditional control at an equivalent average temperature reveals that the MPC maintains a consistently lower power demand throughout the week. The spikes observed in the graph can be explained by the scheduled morning activation of the ventilation system. This startup sequence introduces a cooling load, resulting in a sudden increase in heating demand that the radiators must compensate for to maintain the indoor temperature setpoint. To evaluate the peak shaving performance, the maximum heating power demand was identified for each day during the simulated week. Table 6.6 summarizes the peak reduction achieved by the MPC compared to the traditional control at an equivalent average temperature.

Table 6.6: Daily peak power demand for traditional control and MPC, including the relative reduction for each day.

Day	Peak power [kW] (Traditional control)	Peak power [kW] (MPC: Peak shaving)	Reduction [%]
7	24.34	19.23	21.01%
8	26.25	21.35	18.67%
9	34.65	21.95	36.65%
10	34.48	24.36	29.35%
11	38.34	28.32	26.14%
12	42.10	29.08	30.92%
13	41.06	32.77	20.18%
Avg.	**34.53**	**25.29**	**26.13%**

The results demonstrate a consistent reduction in peak loads with an average reduction of 26% throughout the week. The most significant impact is observed on day 9, where the peak is reduced by 36%. This consistent performance proves the MPC's ability to utilize the building's thermal mass to buffer power demand, effectively smoothing out the peaks that a reactive traditional control system cannot avoid.

6.3.6 Stability during forecast uncertainty

As stated in section 5.5, the forecast uncertainty was evaluated for both weather and occupancy. The evaluation utilized the same MPC settings as for optimizing energy savings. When simulating, the deviating climate file was applied to the MPC and the correct climate file to IDA ICE. The resulting temperature for zone 17 is plotted in Figure 6.8.

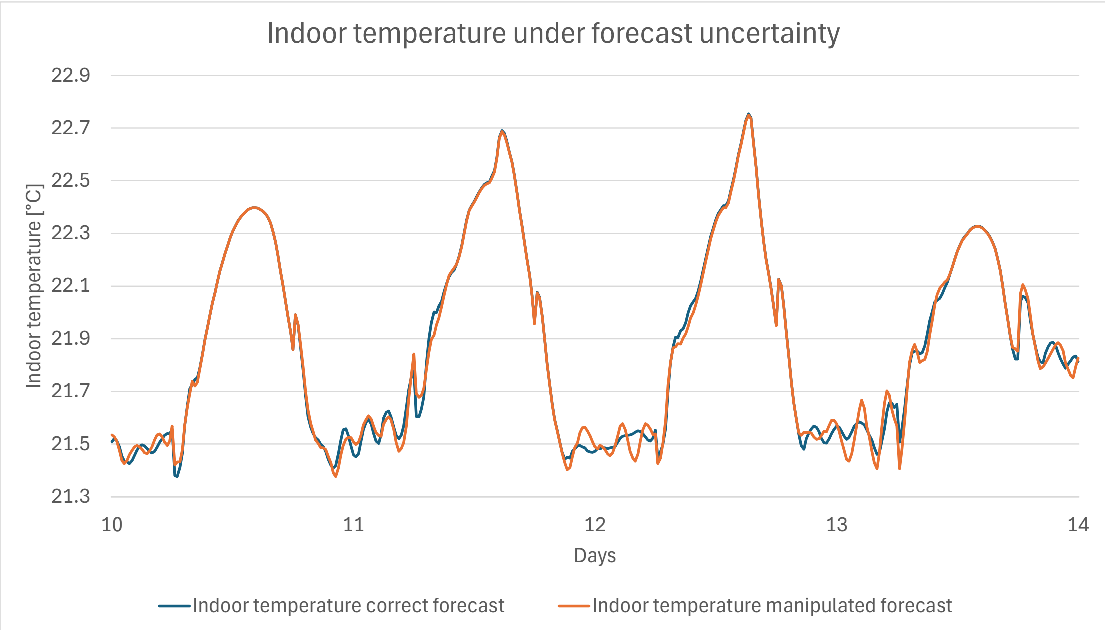

Figure 6.8: Resulting indoor temperature in zone 17 with and without forecast uncertainty for the outside temperature.

As viewable in Figure 6.8, the MPC is resilient and handles the deviating forecast well. Although, some increased fluctuations appear on day 12 and 13 which indicates that the MPC initially provides a supply temperature that is either too high or too low which results in a temperature which it did not anticipate. When provided with feedback, the MPC discovers the resulting temperature offset from the calculated value, forcing it to compensate and fluctuations emerge. Additionally, the temperature is not fluctuating above 22 degrees since the p-controller is activated.

To evaluate the consequences for uncertainties in occupancy, a simulation where the schedule in the offices were reduced by 50% was performed. The resulting indoor temperature for zone 17 is displayed in Figure 6.9.

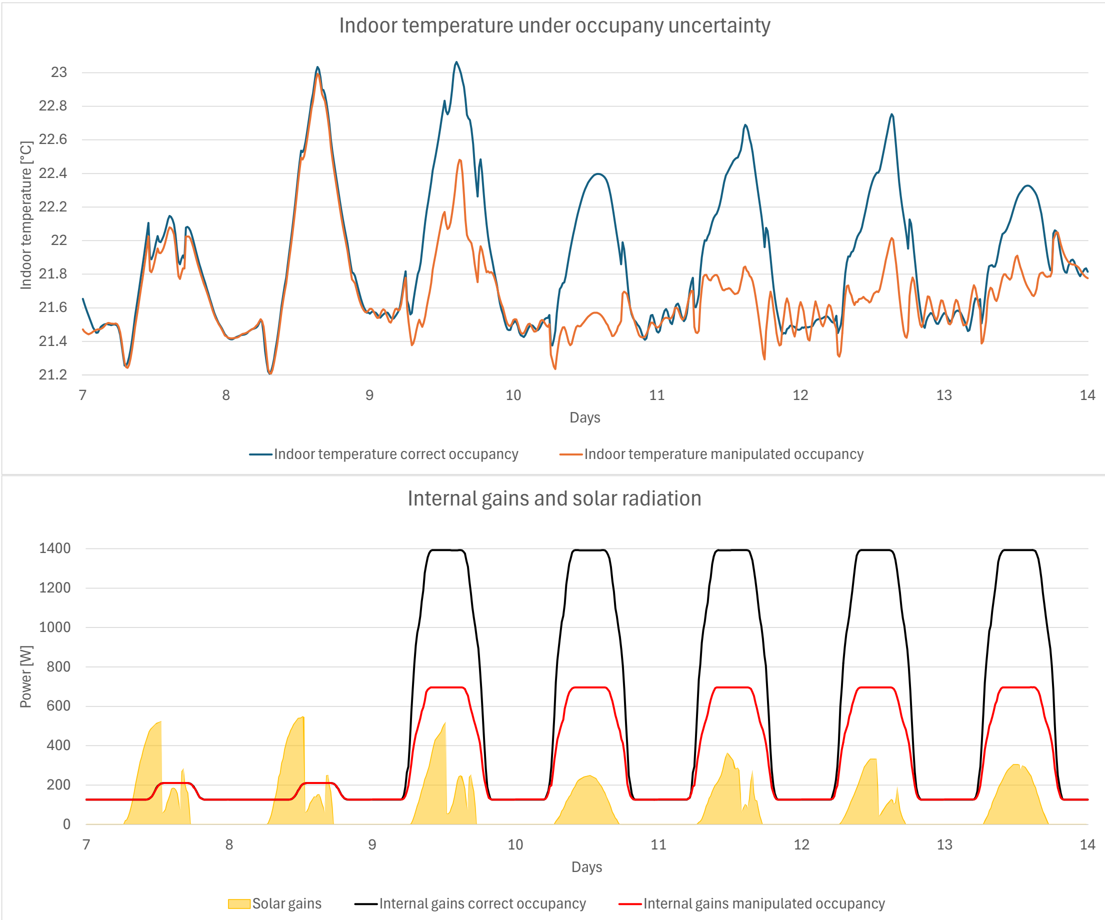

Figure 6.9: Top figure displaying the resulting indoor temperature in zone 17 with and without forecast uncertainty for occupants. Bottom figure displays solar gains accompanied with the internal gains with and without manipulated schedules.

The ocular evaluation of Figure 6.9 reveals that the MPC's overestimation of the internal gains caused it to decrease the supply temperature which yielded a lower indoor temperature. It was also apparent that the fluctuation has increased, which was a consequence of the feedback to the MPC not corresponding with the predicted outcome. To achieve a high-performing MPC, it was concluded that the accuracy of occupant-forecasts are of importance. However, the MPC manages to maintain the indoor temperature in the defined temperature span proving its robustness.

7 Discussion

This chapter evaluates the impact of the identified limitations on the results, alongside an analysis of potential sources of error and the reliability of the state-space models. Furthermore, it provides a critical assessment of the selected control strategy to determine whether its appropriate for the given application. Finally, the chapter concludes by discussing possible directions for future research.

7.1 Limitations

The extent to which the limitations described in Chapter 1 influenced the study remains a subject of analysis. While a two-week simulation period might be perceived as brief, this constraint was necessary because of the substantial computational time of the IDA ICE model. This duration was deemed sufficient to generate representative results within the project's time frame. Since the scope is limited to the heating season, an annual simulation would have been excessive.

Furthermore, while exploring months with peak heating demands remains of interest, March was strategically selected to evaluate the MPC's ability to manage significant solar gains while a substantial heating requirement still exists. However, March is particularly favorable for MPC implementation due to the relatively low heating demand in this reference case. When combining the low heating demand with the utilization of solar radiation through the MPC's predictive capabilities, the resulting performance improvements were of high significance. To comprehensively evaluate the advantages of the MPC framework, the simulation horizon should be extended to evaluate other periods throughout the heating season.

An additional limitation involved the selection of only a subset of zones for the control scheme. This decision was forced by the high complexity of certain areas, where the resulting state-space models exhibited poor fits, making them unsuitable for the control framework. To ensure the robustness of the MPC, zones identified as worst-case scenarios through a thermal analysis of the building were prioritized. However, this selection process introduces the risk of overlooking zones that may become critical under specific conditions. Ideally, a control scheme involving all zones would have been implemented if the project's time frame would have been longer.

7.2 Sources of error

Several sources of error were identified during the implementation of this technology. Primarily, the control strategy is highly dependent on an extensive sensor network and its functionality. A single sensor malfunction can significantly degrade energy efficiency and compromise the entire control scheme.

Furthermore, the impact of forecast uncertainty was thoroughly examined. The MPC showed notable robustness when subjected to a manipulated outdoor temperature, resulting in only minimal indoor fluctuations. It proved to be slightly more sensitive to deviations in occupancy patterns. Specifically, when actual occupancy was lower than predicted, more pronounced temperature deviations occurred. However, it was concluded that an entirely correct forecast is not of critical importance for the system's overall performance.

7.3 The importance of model fit

The MPC relies heavily on the mathematical state-space models when predicting indoor temperatures. A fit percentage of approximately 70% indicates a mismatch between the simplified grey-box model and the IDA ICE environment. This discrepancy affects the MPC's predictive accuracy, meaning the controller cannot rely solely on open-loop predictions but requires continuous feedback to adjust the supply temperature effectively.

The difficulty in achieving a higher fit percentage is based from the fact that a simplified RC-model cannot fully capture the complex thermal dynamics simulated in IDA ICE because of simplifications and non-nonlinearities. Various RC-model configurations of differing complexities were evaluated during the testing phase. However, it was concluded that increasing the number of parameters did not improve the model fit. Instead, the optimization algorithm often became trapped into local minima. Ultimately, an intermediate model structure was selected to optimize the trade-off between prediction accuracy and model complexity. This balanced configuration ensured sufficient reliability for the controller without introducing excessive computational overload. However, it is important to note that while IDA ICE is an advanced tool, it is still a simulation environment and not a perfect representation of reality. Ultimate validation of this control strategy would therefore require implementation in a real building.

A notable limitation of the current methodology is that the state-space models are trained on the same climate profile used in the co-simulation. This represents a perfect information scenario that is unattainable in real-world applications. In reality, the models would have to be trained on the period prior to the simulation period which likely would lead to lower prediction accuracy. To prevent this, a more frequent recalibration strategy could be implemented to enhance accuracy. However, such an approach would increase the computational load as the model parameters would require continuous re-optimization. This strategy is what the most advanced MPC-based services offer on the market.

7.4 Choice of control strategy

Initially, the control strategy was intended to manipulate the individual radiator valve openings in every zone, meaning the predefined supply temperature is kept while the local p-controllers are replaced with MPC. However, following consultations with Algeno AB, the focus was shifted toward optimizing the central supply temperature. Controlling individual valves would not only increase the dimensionality and complexity of the optimization problem but also risk destabilizing the indoor climate by bypassing the local proportional controllers. By adopting this approach, the local P-controllers can effectively manage rapid fluctuations within each zone, while the MPC ensures an optimized supply temperature for the entire building.

Another issue with controlling the valve opening is that most buildings are not equipped with enough sensors that is required when controlling each radiator individually. Although this control strategy would be optimal, controlling each room individually is complicated by unpredictable local disturbances, such as the opening of windows, which an MPC cannot anticipate. Transitioning to a supply temperature control strategy not only enhanced the overall controllability and robustness of the system but also ensured that the findings of this thesis are more applicable to real-world scenarios.

Regarding the implemented control strategy, a reduction in supply temperature requires an increased mass flow rate to maintain the required thermal output. An elevated flow rate increases the energy use of the circulation pumps. However, it could simultaneously affect the COP of the heat pump with the reduction of temperature lift. The net energy impact of these competing factors was not quantified within the scope of this study but would be of interest to determine the overall system efficiency.

7.5 Further research

During the implementation phase, the integration of economic objectives within the MPC framework was explored. It was quickly identified that adding economic factors into the cost function significantly increases the tuning complexity. While many similar commercial products prioritize economic optimization to enhance market appeal, the decision was made to exclude this feature from the current scope. Another valuable economic aspect is the potential for peak shaving. As society undergoes rapid electrification, the ability to reduce peak power demands during high grid loads is becoming increasingly critical. By leveraging the predictive ability of an MPC, unnecessary stress on the power grid could effectively be relieved. However, although an economic MPC approach remains of significant interest for future research, the primary focus of this thesis was maintained on the described research questions.

A significant area for future research involves the detailed modeling of the building's ventilation system. The coexistence of CAV and VAV systems, particularly when integrated with complex cooling control schemes were not possible to fully address within the current project timeframe. A more detailed representation of these airflows would allow the MPC to better anticipate the convective heat transfer and its impact on the overall thermal environment.

Lastly, as concluded in Section 6.3.6, the performance of the MPC is highly sensitive to the accuracy of occupancy forecasts. While this study benefited from detailed, predefined occupancy profiles, acquiring such data poses a significant challenge in a real-world scenario. Future research should therefore explore methods for generating realistic occupancy predictions, such as integrating data from digital room-booking systems or utilizing machine learning algorithms for predictive occupancy modeling.

8 Conclusion

This thesis evaluated the implementation of a model predictive controller in a high complexity, modern office building. The study ran into multiple challenges, starting with the insufficient model fit of the state-space models due to simplifications in the underlying RC-model. This mismatch led to predictive deviations, demonstrating that the MPC is heavily reliant on continuous feedback from measured values. This conclusion led to the introduction of a closed-loop co-simulation environment with IDA ICE.

The results of this study successfully address the research questions outlined in Chapter 1. Evaluation of the MPC's energy performance demonstrated that energy savings of 3–5% were achieved when isolating the impact of the control logic. Regarding peak shaving capabilities, the system delivered an average reduction of 26% in peak power demand during the analyzed week in March. Furthermore, thermal comfort was evaluated through an analysis of the average indoor temperature, which initially revealed that the MPC operated at a lower mean temperature. However, after normalizing for these temperature differences to ensure a baseline comparison, it was concluded that thermal comfort was fully maintained while still yielding improved energy performance. Lastly, system stability under forecast uncertainty was evaluated, demonstrating that the MPC was remarkably robust to outdoor temperature deviations and occupancy inaccuracies.

While model predictive control has been thoroughly researched for many years and a few commercial products are available, the building sector has yet to see a transition away from traditional control systems. This slow adoption remains, despite verified energy savings in available research studies. This is a consequence of the specialized expertise required to deploy and maintain these control systems along with the time-consuming configuration process for each specific building.

As this study was conducted entirely within a simulated environment, validation in a physical building is required to fully strengthen these findings and further explore the practical potential of MPC in the built environment. In conclusion, utilizing MPC to optimize central supply temperatures offers a viable path forward for energy efficiency in modern buildings, successfully demonstrating how advanced control of a hydronic heating system enhances building operations.

9 References

Algeno AB. (2024). Algeno - smart fastighetsautomation [Accessed: 2026-04-22]. https://www.algeno.se/

Al-Sanea, S. A., Zedan, M. F., & Al-Hajri, S. N. (2017). Thermal inertia in buildings: A review of impacts across climate and building use. *Renewable and Sustainable Energy Reviews*, *80*, 1138–1150. https://doi.org/10.1016/j.rser.2017.09.084

ASHRAE. (2022). *Standard 90.1-2022: Energy standard for sites and buildings except low-rise residential buildings* (Standard). American Society of Heating, Refrigerating and Air-Conditioning Engineers. Atlanta, GA.

Boverket. (2017). Boverkets föreskrifter om ändring av verkets föreskrifter och allmänna råd (2016:12) om fastställande av byggnadens energianvändning vid normalt brukande och ett normalår [Retrieved: 2026-04-24].

Boverket. (2024). *Energianvändning i bygg- och fastighetssektorn*. Retrieved January 26, 2026, from https://www.boverket.se/sv/byggande/hallbart-byggande-och-forvaltning/miljoindikatorer---aktuell-status/energianvandning/

Göteborg Energi. (n.d.). Smart styrning – jämna ut din elanvändning [smart control – balance your electricity usage] [Accessed: 2026-01-28]. https://www.goteborgenergi.se/privat/elnat/smart-styrning

Khabbazi, A. J., Pergantis, E. N., Premer, L. D. R., Papageorgiou, P., Lee, A. H., Braun, J. E., Henze, G. P., & Kircher, K. J. (2025). Lessons learned from field demonstrations of model predictive control and reinforcement learning for residential and commercial HVAC: A review. *Applied Energy*, *399*. https://doi.org/10.1016/j.apenergy.2025.126459

Lindelöf, D., Alisafaee, M., Borsò, P., Grigis, C., & Viaene, J. (2018). Bayesian verification of an energy conservation measure. *Energy Buildings*, *171*, 1–10.

Lolli, N., Gorantonaki, E., & Clauß, J. (2024). Predictive heating control and perceived thermal comfort in a Norwegian office building. *Energies*, *17*(15).

Mathworks. (n.d.-a). *What are state-space models?* Mathworks. https://se.mathworks.com/help/ident/ug/what-are-state-space-models.html

Mathworks. (n.d.-b). *What is model predictive control?* Mathworks. Retrieved June 15, 2026, from https://www.mathworks.com/help/mpc/gs/what-is-mpc.html

Myrspoven. (n.d.). *Smarter solutions for sustainable energy*. Myrspoven. Retrieved May 21, 2026, from https://myrspoven.com/sv/solutions/

Olsson, D. (2014). *Modellbaserad styrning av värmesystem baserat på prognostiserat väder* [Licentiat essay]. Chalmers tekniska högskola.

Parisio, A., Fabietti, L., Molinari, M., Varagnolo, D., & Johansson, K. H. (2014). Control of HVAC systems via scenario-based explicit MPC. *Proceedings of the 53rd IEEE Conference on Decision and Control (CDC)*, 5201–5207. https://doi.org/10.1109/CDC.2014.7040202

Petersson, B.-Å. (2014). *Tillämpad byggnadsfysik* (5:2). Studentlitteratur.

Prívara, S., Široký, J., Ferkl, L., & Cigler, J. (2011). Model predictive control of a building heating system: The first experience. *Energy and Buildings*, *43*(2), 564–572.

Sampaio, P. R., Salvazet, R., Mandel, P., Becker, G., & Chenu, D. (2021). Simulation and optimal control of heating and cooling systems: A case study of a commercial building. *Energy & Buildings*, *246*.

Široký, J., Oldewurtel, F., Cigler, J., & Prívara, S. (2011). Experimental analysis of model predictive control for an energy efficient building heating system. *Applied Energy*, *88*(9), 3079–3087.

SMHI. (2025). *Uppföljning av prognoser*. SMHI. https://www.smhi.se/data/temperatur-och-vind/temperatur/uppfoljning-av-prognoser

SMHI. (n.d.-a). *Hur är en numerisk väderprognosmodell uppbyggd?* SMHI. https://www.smhi.se/kunskapsbanken/meteorologi/meteorologiska-modeller/hur-ar-en-numerisk-vaderprognosmodell-uppbyggd

SMHI. (n.d.-b). *Kan man lita på väderprognoser?* SMHI. https://www.smhi.se/kunskapsbanken/meteorologi/vaderprognoser/kan-man-lita-pa-vaderprognoser

Stoffel, P., Berktold, M., & Müller, D. (2024). Real-life data-driven model predictive control for building energy systems comparing different machine learning models. *Energy & Buildings*, *305*.

Sveby. (2010). Brukarindata för energiberäkningar i kontor - vägledning [Retrieved: 2026-04-24].

Svenne Freund, G. S. (2021). Implementation of model predictive control in a large-sized, low-energy office building. *Building and Environment*, *197*.

X. Ding, A. C. (2025). Multi-zone hvac control with model-based deep reinforcement learning. *IEEE TRANSACTIONS ON AUTOMATION SCIENCE AND ENGINEERING*, *22*, 4408–4426.

Z. Liao, A. D. (2010). An inferential model-based predictive control scheme for optimizing the operation of boilers in building space-heating systems. *TRANSACTIONS ON CONTROL SYSTEMS TECHNOLOGY*, *18*(5), 1092–1102.

A Appendix A

The simulations were conducted in IDA ICE 5.1.1 where the input data report of the model is presented below.

EQUA SIMULATION TECHNOLOGY GROUP

Input data Report

Project		**Building**	
		Model floor area	8034.0 m2
Customer		Model volume	32802.0 m3
Created by		Model ground area	858.7 m2
Location	Malmö - Sturup_026360	Model envelope area	7494.0 m2
Climate file	Malmo_Malmo_102105_2025	Window/Envelope	45.4 %
Case		Average U-value	0.6271 W/(m2 K)
Simulated	2026-04-23 16:27:12	Envelope area per Volume	0.2285 m2/m3

Wind driven infiltration airflow rate **3604.432 l/s at 50.000 Pa**

Building envelope	Area [m2]	U [W/(m2 K)]	U*A [W/K]	% of total
Walls above ground	**1600.50**	**0.16**	**252.60**	**5.38**
YV plan 21	92.44	0.16	14.87	0.32
YV fläktrum	97.10	0.21	20.29	0.43
YV plan 12-20	1410.96	0.15	217.40	4.63
Walls below ground	**492.93**	**0.19**	**94.65**	**2.01**
YV mark	492.93	0.19	94.65	2.01
Roof	**791.64**	**0.18**	**138.80**	**2.95**
Tak U=0,1	163.96	0.10	16.66	0.35
Tak U=0,12	369.79	0.12	43.67	0.93
Tak ovan garage	257.88	0.30	78.47	1.67
Floor towards ground	**858.75**	**0.23**	**200.60**	**4.27**
PPM btg 300 mm	858.75	0.23	200.60	4.27
Floor towards amb. air	**351.86**	**0.12**	**42.72**	**0.91**
Golv burspråk	351.86	0.12	42.72	0.91
Windows	**3398.35**	**1.07**	**3642.56**	**77.51**
LT/g/U 69/36/1,3	1562.63	1.30	2031.42	43.23
LT/g/U 46/36/1,3	510.90	1.30	664.17	14.13
LT/g/U 53/27/0,7	386.83	0.70	270.78	5.76
LT/g/U 53/27/0,68	302.19	0.68	205.49	4.37
LT/g/U 62/35/0,77	75.11	0.77	57.84	1.23
LT/g/U 62/35/0,74	64.64	0.74	47.83	1.02
Entre U-2,0	12.56	2.00	25.11	0.53
LT/g/U 62/35/0,72	73.81	0.72	53.14	1.13
LT/g/U 62/35/0,7	409.67	0.70	286.77	6.10
Doors	**0.00**	**0.00**	**0.00**	**0.00**
Thermal bridges			**327.47**	**6.97**
Total	**7494.03**	**0.63**	**4699.40**	**100.00**

Thermal bridges	Area or Length	Avg. Heat conductivity	Total [W/K]
External wall / internal slab	1147.05 m	0.000 W/(m K)	0.000
External wall / internal wall	332.32 m	0.000 W/(m K)	0.000
External wall / external wall	101.08 m	0.043 W/(m K)	4.346
External windows perimeter	3929.18 m	0.048 W/(m K)	188.601
External doors perimeter	0.00 m	0.000 W/(K m)	0.000
Roof / external walls	296.28 m	0.140 W/(m K)	41.479
External slab / external walls	400.34 m	0.250 W/(m K)	100.085
Balcony floor / external walls	0.00 m	0.000 W/(K m)	0.000
External floor towards amb. air / internal wall	11.17 m	0.000 W/(m K)	0.000
Roof / Internal walls	491.44 m	0.000 W/(m K)	0.000
External walls, inner corner	3.88 m	0.000 W/(m K)	0.000
Roof / external walls, inner corner	75.73 m	-0.093 W/(m K)	-7.043
External slab / external walls, inner corner	203.81 m	0.000 W/(m K)	0.000
Total envelope (incl. roof and ground)	7494.03 m^2	0.000 W/(m^2 K)	0.000
Extra losses	-	-	0.000
Sum	-	-	**327.469**

Page 1 of 2

Windows	Area [m2]	U Glass [W/(m2 K)]	U Frame [W/(m2 K)]	U Total [W/(m2 K)]	U*A [W/K]	Shading factor g
N	589.69	0.78	0.76	0.77	456.15	0.34
E	1123.15	1.23	1.23	1.23	1386.05	0.35
S	1134.74	1.21	1.21	1.21	1376.80	0.35
W	550.77	0.77	0.76	0.77	423.56	0.29
Total	3398.35	1.07	1.05	1.07	3642.56	0.34

Air handling unit	Pressure head supply/exhaust [Pa/Pa]	Fan efficiency supply/exhaust [-/-]	System SFP [kW/(m3/s)]	Heat exchanger temp. ratio/min exhaust temp. [-/C]
Plan 09-13 (5701-02)	800.00/800.00	0.80/0.80	1.00/1.00	0.83/-5.00
Plan 14-21 (5701-01)	700.00/690.00	0.70/0.69	1.00/1.00	0.83/-5.00
Avluft/uteluft	0.01/0.01	0.60/0.60	0.00/0.00	0.00/1.00
omklädning (5701-02)	800.00/800.00	0.80/0.80	1.00/1.00	0.83/-5.00

DHW use	kWh/year	Total, [l/s]
	12300.000	0.007

Schedule name	Percentage of zones with this schedule (% of total zone area).
8-17	0.83
Café	1.65
Café/Library	7.04
9-17 vdg	3.91
Occ. custom	44.38
Meeting room	8.94
10-14 vdg	0.49
ALWAYS_ON	32.75

Schedule name	Percentage of zones with this schedule (% of total zone area)
8-17	0.85
Café	1.68
Café/Library	7.19
9-17 vdg	4.00
Tenant electricity	45.32
Meeting room	9.13
ALWAYS_OFF	12.90
10-14 vdg	18.92

Schedule name	Percentage of zones with this schedule (% of total zone area)
8-17	0.83
Café	1.65
Café/Library	7.04
9-17 vdg	3.91
Tenant electricity	44.38
Meeting room	8.94
10-14 vdg	0.49
ALWAYS_OFF	32.75

B Appendix B

Python code to build state-space models

```
# ------------- BUILD GREY BOX MODELS --------------#

import pandas as pd
import numpy as np
import os
import json
from scipy.optimize import minimize
from scipy.signal import StateSpace, lsim
from scipy.interpolate import interp1d
from multiprocessing import Pool, cpu_count

# ---------------------------------------------------------
# 1. Settings
# ---------------------------------------------------------
BASE_PATH = r'C:\Users\c34\Desktop\Matlab\Co-Sim\sim5_training\energy'
CLIM_PATH = r'C:\Users\c34\Desktop\Matlab\Co-Sim\Malmo_klimatfil3.prn'
PRBS_PATH = r'C:\Users\c34\Desktop\Matlab\Co-Sim\PRBS_framledning_15min.prn'

ZONES_TO_TRAIN = [
    'zone 85', 'zone 77', 'zone 35', 'zone 69', 'zone 61', 'zone 25',
    'zone 59', 'zone 49', 'zone 18', 'zone 84', 'zone 76', 'zone 30',
    'zone 68', 'zone 60', 'zone 24', 'zone 56', 'zone 48', 'zone 17'
]

# ---------------------------------------------------------
# 2. Physical model & target function
# ---------------------------------------------------------
def simulate_rc_plant_solar(params, Ta, Q_known, I_solar, T_sup, dt, Ti_0):
    R_ei, R_leak, R_e, C_i, C_e, f_mass, T_e0, Q_bias, K_rad, A_win_eff = params
    Q_conv = Q_known + (1 - f_mass) * (I_solar * A_win_eff) + Q_bias
    Q_rad = f_mass * (I_solar * A_win_eff)

    A = np.array([[-(1/R_ei + 1/R_leak + K_rad)/C_i, 1/(R_ei*C_i)],
                  [1/(R_ei*C_e), -(1/R_ei + 1/R_e)/C_e]])
    B = np.array([[1/(R_leak*C_i), 1/C_i, 0, K_rad/C_i],
                  [1/(R_e*C_e), 0, 1/C_e, 0]])

    sys = StateSpace(A, B, np.array([[1, 0]]), np.array([[0, 0, 0, 0]]))
    U = np.column_stack((Ta, Q_conv, Q_rad, T_sup))
    _, y, _ = lsim(sys, U, np.arange(len(Ta)) * dt, X0=[Ti_0, T_e0])
    return y.flatten()

def objective_solar(scale_factors, base_guess, Ta, Q_known, I_solar,
                    T_sup, Ti_measured, dt, skip_steps):
    p = scale_factors * base_guess
    Ti_0 = Ti_measured[0]

    # Pack 9 parameters into the 10 required for simulation (Te0 locked to Ti0)
    full_params = [p[0], p[1], p[2], p[3], p[4], p[5], Ti_0, p[6], p[7], p[8]]

    if np.any(p[:6] <= 0) or p[7] <= 0 or p[8] <= 0: return 1e15

    Ti_sim = simulate_rc_plant_solar(full_params, Ta, Q_known,
                                     I_solar, T_sup, dt, Ti_0)
    return np.mean((Ti_sim[skip_steps:] - Ti_measured[skip_steps:])**2)

# ---------------------------------------------------------
# 3. Worker-function
# ---------------------------------------------------------
def train_zone_worker(args):
    zone_name, df_prbs, clim_data = args
```

1

```python
f_tair, f_idir, f_idiff = clim_data

try:
    # Load data
    df_temp = pd.read_csv(os.path.join(BASE_PATH,
                                       f'{zone_name}.TEMPERATURES.prn'),
                          sep=r'\s+', comment='#', names=['time',
                                                          'order',
                                                          'tairmean',
                                                          'top'])
    e_cols = ['time', 'order', 'q_cool', 'q_equip', 'q_heat',
              'q_light', 'q_loss', 'q_occ', 'qintw', 'ql_a',
              'qventil', 'qwcb', 'qwind']
    df_energy = pd.read_csv(os.path.join(BASE_PATH,
                                         f'{zone_name}.ZONE-ENERGY.prn'),
                            sep=r'\s+', comment='#', names=e_cols)

    df = pd.merge(df_temp[['time', 'tairmean']], df_energy, on='time')
    df['Tair'] = f_tair(df['time'])
    df['I_solar'] = f_idir(df['time']) + f_idiff(df['time'])
    df = pd.merge(df, df_prbs[['time', 'T_supply']], on='time')
    df['Q_known'] = (df['q_cool'] + df['q_occ'] + df['q_equip'] +
                     df['q_light'] + df['qintw'] + df['ql_a'] +
                     df['qventil'])

    dt = (df['time'].iloc[1] - df['time'].iloc[0]) * 3600

    # Spin-up (1 week)
    start_mars = 1416
    spin_up_h = 72
    skip_steps = int(spin_up_h * (3600/dt))
    df_train = df[(df['time'] >= (start_mars - spin_up_h)) &
                  (df['time'] <= 1753)].reset_index(drop=True)

    # Optimization (9 parameters)
    base_guess = np.array([0.006, 0.03, 0.03, 2.5e6, 8.0e7, 0.5,
                           10.0, 100.0, 5.0])
    initial_scale = np.ones(9)
    abs_bounds = [
        (1e-3, 0.01), (1e-3, 0.1), (1e-3, 0.1), # R-values
        (8e5, 2e7), (3e7, 7e8),                 # C-values
        (0.1, 0.9),                             # f_mass
        (-200.0, 400.0),                        # Q_bias
        (90.0, 170.0),                          # K_rad
        (0.5, 35.0)                             # A_win_eff
    ]
    bounds = [(low/g, high/g) for (low, high), g in zip(abs_bounds,
                                                         base_guess)]

    res = minimize(objective_solar, initial_scale,
                   args=(base_guess, df_train['Tair'].values,
                         df_train['Q_known'].values,
                         df_train['I_solar'].values,
                         df_train['T_supply'].values,
                         df_train['tairmean'].values, dt, skip_steps),
                   method='L-BFGS-B', bounds=bounds)

    # Result handling
    opt_p = res.x * base_guess
    Ti_0 = df_train['tairmean'].iloc[0]
    full_opt_params = [opt_p[0], opt_p[1], opt_p[2], opt_p[3], opt_p[4],
```

2

```
                    opt_p[5], Ti_0, opt_p[6], opt_p[7], opt_p[8]]

        Ti_sim_total = simulate_rc_plant_solar(full_opt_params,
                                               df_train['Tair'].values,
                                               df_train['Q_known'].values,
                                               df_train['I_solar'].values,
                                               df_train['T_supply'].values,
                                               dt, Ti_0)

        y_sim = Ti_sim_total[skip_steps:]
        y_true = df_train['tairmean'].values[skip_steps:]
        rmse = np.sqrt(np.mean((y_true - y_sim)**2))
        fit = (1 - (np.linalg.norm(y_true - y_sim) /
                    np.linalg.norm(y_true - np.mean(y_true)))) * 100

        # Save JSON
        keys = ['R_ie', 'R_ia', 'R_ea', 'C_i', 'C_e', 'f_mass',
                'T_e0', 'Q_bias', 'K_rad', 'A_win_eff']
        p_dict = {k: float(v) for k, v in zip(keys, full_opt_params)}
        with open(os.path.join(BASE_PATH, f'greybox_params_{zone_name}.json'),
                  'w') as f:
            json.dump(p_dict, f, indent=4)

        return {"name": zone_name, "fit": fit, "rmse": rmse,
                "status": "success"}

    except Exception as e:
        return {"name": zone_name, "status": "error", "error": str(e)}

# --------------------------------------------------------
# 4. Main Program
# --------------------------------------------------------
if __name__ == '__main__':
    print("--- TRAINING STARTING ---")
    print("Loading global files...")

    df_clim_raw = pd.read_csv(CLIM_PATH, sep=r'\s+', comment='#',
                              names=['time', 'Tair', 'RelHum', 'WindX',
                                     'WindY', 'IDirNorm', 'IDiffHor',
                                     'Skycover'])
    df_prbs = pd.read_csv(PRBS_PATH, sep='\t', comment='#', names=['time',
                                                                   'T_supply'])

    f_tair = interp1d(df_clim_raw['time'], df_clim_raw['Tair'],
                      kind='linear', fill_value="extrapolate")
    f_idir = interp1d(df_clim_raw['time'], df_clim_raw['IDirNorm'],
                      kind='linear', fill_value="extrapolate")
    f_idiff = interp1d(df_clim_raw['time'], df_clim_raw['IDiffHor'],
                       kind='linear', fill_value="extrapolate")

    tasks = [(z, df_prbs, (f_tair, f_idir, f_idiff)) for z in ZONES_TO_TRAIN]
    num_workers = max(1, cpu_count() - 1)

    print(f"Training {len(ZONES_TO_TRAIN)} zones on {num_workers} cores...")
    print(f"{'ZONE NAME':<15} | {'FIT (%)':<10} | {'RMSE (°C)':<10} | STATUS")
    print("-" * 60)
```

3

Python code to run the co-simulation

```
# ------------- MPC CO-SIMULATION --------------#

import ctypes
import numpy as np
import pandas as pd
import cvxpy as cp
import matplotlib.pyplot as plt
import sys
import os
import json
from scipy.signal import StateSpace
from scipy.interpolate import interp1d

# ========================================================================
# 0. CONFIGURATION AND PATHS
# ========================================================================
base_path = r'C:\Users\c34\Desktop\Matlab\Co-Sim\sim5_training\energy'
base_path2 = r'C:\Users\c34\Desktop\Matlab\Co-Sim'
clim_path = os.path.join(base_path2, 'Malmo_klimatfil3.prn')

START_DAY = 60
SIM_DAYS = 14
DT_SEC = 900  # 15 minutes in seconds
DT_HOURS = DT_SEC / 3600
START_IDX_OFFSET = int((START_DAY - 1) * 24 / DT_HOURS)

def get_discrete_greybox_solar(params, dt_sec):
    R_ie, R_ia, R_ea, C_i, C_e, f_mass, T_e0, Q_bias, K_rad, A_win_eff = params

    A_c = np.array([
        [-(1/R_ie + 1/R_ia + K_rad)/C_i, 1/(R_ie*C_i)],
        [1/(R_ie*C_e), -(1/R_ie + 1/R_ea)/C_e]
    ])
    B_full_c = np.array([
        [1/(R_ia*C_i), 1/C_i, 0, K_rad/C_i],
        [1/(R_ea*C_e), 0, 1/C_e, 0]
    ])
    C_c = np.array([[1.0, 0.0]])
    D_c = np.zeros((1, 4))

    sys_c = StateSpace(A_c, B_full_c, C_c, D_c)
    sys_d = sys_c.to_discrete(dt_sec)

    E_d = sys_d.B[:, 0:3]
    B_d = sys_d.B[:, 3:4]

    return sys_d.A, B_d, E_d, sys_d.C, f_mass, Q_bias, A_win_eff

# ========================================================================
# 1. BUILD GREY-BOX MODEL
# ========================================================================
# Zones to control
zone_names = [
    'zone 85', 'zone 77', 'zone 35', 'zone 69', 'zone 61', 'zone 25',
    'zone 59', 'zone 49', 'zone 18', 'zone 84', 'zone 76', 'zone 30',
    'zone 68', 'zone 60', 'zone 24', 'zone 56', 'zone 48', 'zone 17'
]


num_zones = len(zone_names)
zones = []
```

1

```
print(f"Loading {num_zones} zones...")

# --- 1. READ CLIMATE FILE (Common for all zones) ---
df_clim = pd.read_csv(clim_path, sep='\s+', comment='#',
                      names=['time', 'Ta', 'RelHum', 'WindX', 'WindY',
                             'IDirNorm', 'IDiffHor', 'Skycover'])

time_hours_full = np.arange(0, 8761, DT_HOURS)
Ta_interp = interp1d(df_clim['time'], df_clim['Ta'], bounds_error=False,
                     fill_value="extrapolate")(time_hours_full)
I_solar_raw = df_clim['IDirNorm'] + df_clim['IDiffHor']
I_solar_interp = interp1d(df_clim['time'], I_solar_raw, bounds_error=False,
                          fill_value="extrapolate")(time_hours_full)

# --- 2. LOOP THROUGH AND BUILD EACH ZONE ---
for z_name in zone_names:
    # A. Read physical parameters
    params_path = os.path.join(base_path, f'greybox_params_{z_name}.json')
    with open(params_path, 'r') as f:
        loaded_params = json.load(f)

    opt_params = [
        loaded_params['R_ie'], loaded_params['R_ia'], loaded_params['R_ea'],
        loaded_params['C_i'],  loaded_params['C_e'],  loaded_params['f_mass'],
        loaded_params['T_e0'], loaded_params['Q_bias'],
        loaded_params['K_rad'],loaded_params['A_win_eff']
    ]

    # B. Read energy file (Internal loads) for the specific zone
    energy_path = os.path.join(base_path, f'{z_name}.ZONE-ENERGY.prn')
    df_energy = pd.read_csv(energy_path, sep='\s+', comment='#',
                            names=['time', 'order', 'q_cool', 'q_equip',
                                   'q_heat', 'q_light', 'q_loss', 'q_occ',
                                   'qintw', 'ql_a', 'qventil', 'qwcb',
                                   'qwind'])

    Q_known_raw =  df_energy['q_occ'] + df_energy['q_equip']
    + df_energy['q_light']
    Q_known_interp = interp1d(df_energy['time'],
                              Q_known_raw, bounds_error=False,
                              fill_value="extrapolate")(time_hours_full)

    # C. Build State-Space and disturbance matrix
    A_d, B_d, E_d, C_d, f_mass, Q_bias, A_win_eff = get_discrete_greybox_solar
    (opt_params, DT_SEC)

    Q_solar_total = I_solar_interp * A_win_eff
    Q_conv = Q_known_interp + (1 - f_mass) * Q_solar_total + Q_bias
    Q_rad = f_mass * Q_solar_total
    v_data_matrix = np.column_stack((Ta_interp, Q_conv, Q_rad))

    # D. Save zone to list
    zones.append({
        'name': z_name,
        'A': A_d, 'B': B_d, 'E': E_d, 'C': C_d,
        'v_data': v_data_matrix,
        'x_state': np.array([[21.0], [21.0]]),
        'current_bias': 0.0
    })
```

2

```
    print(f" -> {z_name} ready! (K_rad: {loaded_params['K_rad']:.1f},"
          " A_win: {A_win_eff:.2f} m²)")

weight_profile = {'cost_temp': 20.0, 'cost_T_supp': 800,
                  'cost_dT': 600, 'slack': 10000}

# ========================================================================
# 2. BUILD THE GLOBAL MPC PROBLEM
# ========================================================================
p = 40  # Horizon (steps)
print("Building the global MPC problem...")

T_supp = cp.Variable((1, p))
dT_supp = cp.Variable((1, p))
T_supp_prev = cp.Parameter(1)

cost = 0
constraints = [T_supp[0, 0] == T_supp_prev[0] + dT_supp[0, 0]]
for k in range(1, p): constraints += [T_supp[0, k] == T_supp[0, k-1]
                                      + dT_supp[0, k]]

constraints += [T_supp >= 23.0, T_supp <= 45.0]

for k in range(p):
    # Electricity price cost logic removed
    cost += weight_profile['cost_T_supp'] * T_supp[0, k]
    cost += weight_profile['cost_dT'] * cp.square(dT_supp[0, k])

x_inits, v_futures, biases = [], [], []
for z in zones:
    nx, nv = z['A'].shape[0], z['E'].shape[1]
    x_init = cp.Parameter((nx, 1))
    v_future = cp.Parameter((nv, p))
    bias = cp.Parameter(1)
    x_inits.append(x_init); v_futures.append(v_future); biases.append(bias)

    x_var = cp.Variable((nx, p+1))
    slack_low = cp.Variable((1, p))
    slack_high = cp.Variable((1, p))

    constraints += [x_var[:, 0:1] == x_init]
    for k in range(p):
        constraints += [x_var[:, k+1:k+2] == z['A'] @ x_var[:, k:k+1]
                        + z['B'] * T_supp[0, k] + z['E'] @ v_future[:, k:k+1]]
        y_pred = z['C'] @ x_var[:, k+1:k+2] + bias

        constraints += [y_pred >= 21 - slack_low[0, k],
                        y_pred <= 25.0 + slack_high[0, k]]
        constraints += [slack_low[0, k] >= 0, slack_high[0, k] >= 0]
        cost += weight_profile['slack'] * slack_low[0, k]
        + (weight_profile['slack']/10) * slack_high[0, k]
        cost += weight_profile['cost_temp'] * cp.pos(y_pred - 22.3)
        cost += weight_profile['cost_temp'] * cp.pos(21.9 - y_pred)

global_prob = cp.Problem(cp.Minimize(cost), constraints)
last_T_supp = 40.0

# ========================================================================
# 3. IDA ICE COUPLING
# ========================================================================
mydll = ctypes.CDLL(r'C:\Users\c34\Desktop\Matlab\Co-Sim\idalibN.dll')
```

```python
mydll.CreateStorage.restype = ctypes.c_longlong
try: mydll.CloseAllStorage()
except: pass

VarInterp = ctypes.c_double(0)
import_h = mydll.CreateStorage(b'ICE_zone', num_zones, 1, 0,
                              ctypes.byref(VarInterp), 0)
export_h = mydll.CreateStorage(b'ICE_heatCtr', 1, 1, 1850,
                              ctypes.byref(VarInterp), 0)
if import_h <= 0: print("Could not connect to IDA ICE!"); sys.exit()

# =========================================================================
# 4. SIMULATION LOOP
# =========================================================================
time_history, T_supp_history = [], []
temp_history = [[] for _ in range(num_zones)]
solar_history = [[] for _ in range(num_zones)]
outdoor_temp_history = []     # Store outdoor temp
ctrl_zone_history = [] # Store which zone is controlling
internal_load_history = []
t = 0.0
n = SIM_DAYS * int(3600 / DT_SEC) * 24 + 1
print(f"Starting Global Grey-Box MPC. Starting on day {START_DAY}...")

for i in range(n):
    d_vals = (ctypes.c_double * num_zones)()
    mydll.RetrieveStoredData(ctypes.c_longlong(import_h),
                            ctypes.c_double(t), d_vals)
    y_currents = [val if val > 10 else 21.0 for val in d_vals]
    current_hour = t / 3600.0

    T_supp_prev.value = np.array([last_T_supp])

    # 1. Update state for each zone
    for z_idx, z in enumerate(zones):
        y_now = y_currents[z_idx]
        model_guess = (z['C'] @ z['x_state']).item()
        z['current_bias'] = y_now - model_guess

        x_inits[z_idx].value = z['x_state']
        biases[z_idx].value = np.array([z['current_bias']])

        vf = np.zeros((z['E'].shape[1], p))
        for s in range(p):
            idx = min(START_IDX_OFFSET + i + s, len(z['v_data']) - 1)
            vf[:, s] = z['v_data'][idx, :]
        v_futures[z_idx].value = vf

    # 2. Solve the global optimization problem
    try:
        global_prob.solve(solver=cp.SCS, max_iters=5000, eps=1e-4)
        if global_prob.status in [cp.OPTIMAL, cp.OPTIMAL_INACCURATE]:
            opt_T_supp = float(T_supp.value[0, 0])
        else:
            opt_T_supp = min(45.0, last_T_supp + 1.0)
            print(f" HOUR {t/3600:.1f}: Solver gave up!"
                  " Backup: {opt_T_supp:.1f} °C")
    except Exception as e:
        opt_T_supp = min(45.0, last_T_supp + 1.0)
        print(f" HOUR {t/3600:.1f}: Solver crashed! Backup:"
              " {opt_T_supp:.1f} °C")
```

4

```python
    # 3. State Update and Logging
    predicted_temps = []
    for z_idx, z in enumerate(zones):
        z['x_state'] = z['A'] @ z['x_state'] + z['B'] * opt_T_supp
        + z['E'] @ v_futures[z_idx].value[:, 0:1]
        temp_history[z_idx].append(y_currents[z_idx])

        safe_idx = min(START_IDX_OFFSET + i, len(I_solar_interp) - 1)
        solar_history[z_idx].append(I_solar_interp[safe_idx])

        y_next = (z['C'] @ z['x_state']).item() + z['current_bias']
        predicted_temps.append(y_next)

    safe_idx_ext = min(START_IDX_OFFSET + i, len(Ta_interp) - 1)
    outdoor_temp_history.append(Ta_interp[safe_idx_ext])

    q_int = zones[0]['v_data'][safe_idx_ext, 1]
    internal_load_history.append(q_int)

    controlling_idx = np.argmin(predicted_temps)
    controlling_name = zones[controlling_idx]['name']
    ctrl_zone_history.append(controlling_idx)
    controlling_temp_now = y_currents[controlling_idx]

    T_supp_history.append(opt_T_supp)
    time_history.append(current_hour)
    last_T_supp = opt_T_supp

    # Send data to IDA ICE
    out_vals = (ctypes.c_double * 1)(opt_T_supp)
    mydll.StoreData(ctypes.c_longlong(export_h),
                    ctypes.c_double(t + DT_SEC), out_vals, 0)

    if i % 10 == 0:
        print(f"T: {current_hour:4.1f}h | Boiler: {opt_T_supp:4.1f}°C | "
              f"Control on: {controlling_name:8s} "
              "| Temp: {controlling_temp_now:.2f}°C")

    t = round(t + DT_SEC)

# %%
# =========================================================================
# 5. MPC DIAGNOSTICS: INDOOR, BOILER & WEATHER (TWIN Y-AXIS)
# =========================================================================
start_day, end_day = 1, 14
start_hour, end_hour = start_day * 24, end_day * 24

t_arr = np.array(time_history)
mask = (t_arr >= start_hour) & (t_arr <= end_hour)
t_plot_days = t_arr[mask] / 24

fig, (ax1, ax2, ax3) = plt.subplots(3, 1, sharex=True, figsize=(13, 10))
cmap = plt.get_cmap('tab20')

for z_idx, z_name in enumerate(zone_names):
    current_color = cmap(z_idx % 20)
    ax1.plot(t_plot_days, np.array(temp_history[z_idx])[mask],
             color=current_color, label=f'{z_name}', linewidth=1.5)

ax1.axhline(21.0, color='red', linestyle='--', alpha=0.3)
```

5

```python
ax1.set_ylabel('Indoor Temp (°C)')
ax1.set_title(f'MPC Diagnostics: Day {start_day} to {end_day}', fontsize=14)
ax1.grid(True, alpha=0.2)
ax1.legend(loc='upper right', fontsize='small', ncol=2)

# --- Subplot 2: Supply Temperature (Boiler) & Controlling Zone ---
ax2.plot(t_plot_days, np.array(T_supp_history)[mask], color='darkred',
         drawstyle='steps-post', linewidth=2)

if 'ctrl_zone_history' in locals() or 'ctrl_zone_history' in globals():
    ctrl_data = np.array(ctrl_zone_history)[mask]
    for k in range(len(t_plot_days)-1):
        zone_idx = int(ctrl_data[k])
        c_bg = cmap(zone_idx % 20)
        ax2.axvspan(t_plot_days[k], t_plot_days[k+1], color=c_bg, alpha=0.1)

ax2.set_ylabel('Boiler (T_supp °C)')
ax2.set_ylim(20, 45)
ax2.grid(True, alpha=0.2)

# --- Subplot 3: Weather (Outdoor Temp + Solar on Twin Axis) ---
ax3.plot(t_plot_days, np.array(outdoor_temp_history)[mask], color='seagreen',
         label='Outdoor Temp', linewidth=1.5)
ax3.set_ylabel('Outdoor Temp (°C)', color='seagreen')
ax3.tick_params(axis='y', labelcolor='seagreen')
ax3.grid(True, alpha=0.2)

ax3_sol = ax3.twinx()
ax3_sol.plot(t_plot_days, np.array(solar_history[0])[mask], color='goldenrod',
             label='Solar', alpha=0.8)
ax3_sol.fill_between(t_plot_days, np.array(solar_history[0])[mask],
                     color='goldenrod', alpha=0.1)
ax3_sol.set_ylabel('Solar Radiation (W/m²)', color='goldenrod')
ax3_sol.tick_params(axis='y', labelcolor='goldenrod')

lines, labels = ax3.get_legend_handles_labels()
lines2, labels2 = ax3_sol.get_legend_handles_labels()
ax3_sol.legend(lines + lines2, labels + labels2, loc='upper right',
               fontsize='small')

ax3.set_xlabel('Time (Days)')

plt.tight_layout()
plt.show()
```

6

C Appendix C

Optimized parameters for each grey box model of every zone together with hand calculated values as a comparison.

Zone	R_ei [K/W]	R_leak [K/W]	R_e [K/W]	C_i [J/K]	C_e [J/K]	f_mass	T_e0 [°C]	Q_bias [W]	K_rad	A_win_eff [m^2]
Real values	*4.24E-03*	-	*5.02E-02*	*4.75E+05*	*4.36E+07*	-	-	-	-	-
17	5.22E-03	2.09E-02	1.23E-02	2.98E+06	1.36E+08	0.9	26.5	9.7	141.8	11.5
18	5.32E-03	1.70E-02	5.19E-02	3.04E+06	5.10E+07	0.6	26.3	104.7	141.7	3.1
24	5.22E-03	2.37E-02	1.16E-02	3.46E+06	1.67E+08	0.9	26.7	10.0	136.5	13.9
25	7.61E-03	2.25E-02	4.53E-02	2.86E+06	1.03E+08	0.7	26.5	10.0	121.5	5.2
30	4.36E-03	2.41E-02	8.72E-03	4.32E+06	2.22E+08	0.9	26.9	9.8	140.3	19.2
35	6.65E-03	2.42E-02	1.35E-02	3.30E+06	3.21E+08	0.9	26.7	13.1	119.1	15.7
48	3.47E-03	2.38E-02	9.34E-03	4.10E+06	1.80E+08	0.9	27.0	9.5	161.1	15.3
49	5.50E-03	2.02E-02	4.60E-02	3.10E+06	6.56E+07	0.7	26.8	76.3	139.2	3.8
56	4.97E-03	2.24E-02	1.19E-02	3.26E+06	1.46E+08	0.9	26.7	9.6	145.8	13.0
59	7.28E-03	2.04E-02	9.48E-02	2.68E+06	4.67E+07	0.6	26.5	10.7	130.9	3.0
60	4.92E-03	2.32E-02	1.04E-02	3.63E+06	1.88E+08	0.9	26.8	9.9	139.9	15.8
61	7.06E-03	2.20E-02	4.86E-02	2.95E+06	9.85E+07	0.7	26.6	10.0	124.2	5.1
68	3.96E-03	2.23E-02	8.44E-03	4.15E+06	2.09E+08	0.9	26.7	9.6	152.3	19.1
69	6.36E-03	2.17E-02	2.39E-02	3.18E+06	1.69E+08	0.8	26.5	10.8	128.8	9.1
76	4.20E-03	2.43E-02	8.27E-03	4.39E+06	2.23E+08	0.9	26.7	9.7	142.7	19.7
77	5.77E-03	2.33E-02	1.17E-02	3.62E+06	3.50E+08	0.9	26.5	10.4	125.7	17.7
84	5.86E-03	2.11E-02	1.08E-02	3.61E+06	1.96E+08	0.9	25.1	-171.4	121.5	16.8
85	5.36E-03	1.83E-02	1.08E-02	3.79E+06	3.16E+08	0.9	24.9	5.8	126.2	17.8

D Appendix D

Sensible energy balance of traditional control and the MPC energy saving scenario.

Traditional control [W]

Envelope & Thermal bridges	Internal Walls and Masses	Window & Solar	Mech, supply air	Infiltration & Openings	Occupants	Equipment	Light	Local heating units
-3214	1581	-4117	-6144	-1497	4156	1958	2055	5186

MPC: Energy saving [W]

Envelope & Thermal bridges	Internal Walls and Masses	Window & Solar	Mech, supply air	Infiltration & Openings	Occupants	Equipment	Light	Local heating units
-2871	2057	-3901	-5517	-1463	4159	1958	2055	3483

Difference [W]

Envelope & Thermal bridges	Internal Walls and Masses	Window & Solar	Mech, supply air	Infiltration & Openings	Occupants	Equipment	Light	Local heating units
343	476	216	627	34	3	0	0	-1703
20%	28%	13%	37%	2%	-	-	-	-

Traditional control with lower setpoint [W]

Envelope & Thermal bridges	Internal Walls and Masses	Window & Solar	Mech. supply air	Infiltration & Openings	Occupants	Equipment	Light	Local heating units
-3101	1946	-3878	-5357	-1479	4162	1958	2055	3656

MPC: Energy saving [W]

Envelope & Thermal bridges	Internal Walls and Masses	Window & Solar	Mech, supply air	Infiltration & Openings	Occupants	Equipment	Light	Local heating units
-2871	2057	-3901	-5517	-1463	4159	1958	2055	3483

Difference [W]

Envelope & Thermal bridges	Internal Walls and Masses	Window & Solar	Mech, supply air	Infiltration & Openings	Occupants	Equipment	Light	Local heating units
230	111	-23	-160	16	-3	0	0	-173
64%	31%	12%	86%	4%	-	-	-	-

DEPARTMENT OF ARCHITECTURE AND
CIVIL ENGINEERING
CHALMERS UNIVERSITY OF TECHNOLOGY
Gothenburg, Sweden 2026
www.chalmers.se

AVANCEZ
1829

CHALMERS
UNIVERSITY OF TECHNOLOGY